Department of Automation and Systems Technology

Hybrid Microassembly with Surface Tension Driven Self-alignment: Handling Strategies and Micro-fabricated Patterns

Bo Chang

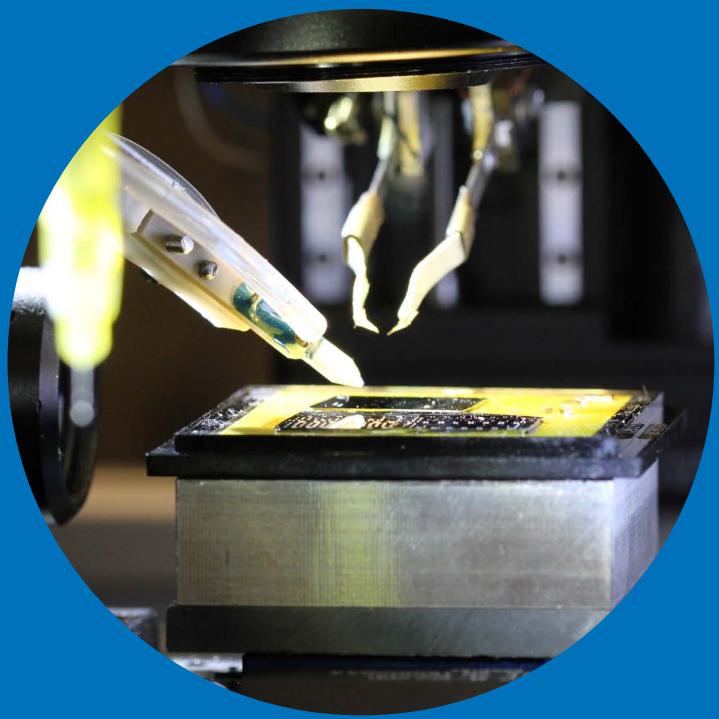

Aalto University

DOCTORAL DISSERTATIONS

Bo Chang

Hybrid Microassembly with Surface Tension Driven Self-alignment: Handling Strategies and Micro-fabricated Patterns

Aalto University

Aalto University publication series
DOCTORAL DISSERTATIONS 117/2013

Hybrid Microassembly with Surface Tension Driven Self-alignment: Handling Strategies and Micro-fabricated Patterns

Bo Chang

A doctoral dissertation completed for the degree of Doctor of Science in Technology to be defended, with the permission of the Aalto University School of Electrical Engineering, at a public examination held in Auditorium AS1 of the school on the 23rd of August 2013 at 12 noon.

Aalto University
School of Electrical Engineering
Department of Automation and Systems Technology
Micro- and Nanorobotics Group

Supervising professor
Professor Heikki Koivo

Thesis advisor
Assistant Professor Quan Zhou

Preliminary examiners
Professor Stéphane Régnier, University of Pierre and Marie Curie, France
Associate Professor Marcel Tichem, Delft University of Technology, The Netherlands

Opponents
Professor Stéphane Régnier, University of Pierre and Marie Curie, France
Assistant Professor Pierre Lambert, Université libre de Bruxelles, Belgium

Aalto University publication series
DOCTORAL DISSERTATIONS 117/2013

ISBN 978-952-60-5261-8 (printed)
ISBN 978-952-60-5262-5 (pdf)
ISSN-L 1799-4934
ISSN 1799-4934 (printed)
ISSN 1799-4942 (pdf)
http://urn.fi/URN:ISBN:978-952-60-5262-5

http://lib.tkk.fi/Diss/

Unigrafia Oy
Helsinki 2013

Finland

Publication orders (printed book):
bo.chang@aalto.fi

Aalto University

Abstract

Aalto University, P.O. Box 11000, FI-00076 Aalto www.aalto.fi

Author
Bo Chang

Name of the doctoral dissertation
Hybrid Microassembly with Surface Tension Driven Self-alignment: Handling Strategies and Micro-fabricated Patterns

Publisher School of Electrical Engineering

Unit Department of Automation and Systems Technology

Series Aalto University publication series DOCTORAL DISSERTATIONS 117/2013

Field of research Control Engineering

Manuscript submitted 18 April 2013 **Date of the defence** 23 August 2013

Permission to publish granted (date) 14 June 2013 **Language** English

☐ **Monograph** ☒ **Article dissertation (summary + original articles)**

Abstract

Hybrid microassembly combines self-assembly technology with traditional robotic pick-and-place technology or other robotic feeding mechanics to construct microsystems. In a typical hybrid microassembly process, a micro part is brought adjacent to the assembly site by a robot handling tool at a high speed but with a relatively low precision, and liquid droplets dispensed by a dispenser at the assembly site align the part at a higher precision. By combing both the robotic pick-and-place technique and self-assembly technique, hybrid microassembly technique can achieve high speed and high precision simultaneously.

This thesis explores the adaptability of hybrid microassembly technique by investigating different hybrid microassembly methods and different types of the patterns. Three hybrid microassembly approaches have been investigated: 1) droplet assisted hybrid microassembly, 2) water mist induced hybrid microassembly and 3) hybrid microassembly with forced wetting. The droplet assisted hybrid microassembly has been studied using patterns with segments and patterns with jagged edges. Parallel microassembly of microchips with water mist induced hybrid microassembly has also been explored. Hybrid microassembly on hydrophobic receptor site with super-hydrophobic substrate has been experimentally investigated with two forced wetting techniques.

Four different types of patterns have been investigated for hybrid microassembly technique: (a) oleophilic/phobic patterns, (2) hydrophobic/super-hydrophobic patterns, (3) segmented patterns and (4) patterns with jagged edges. Hybrid microassembly has been studied on a new patterned oleophilic/oleophobic surface using adhesive droplet in ambient air environment. A patterned hydrophobic/super-hydrophobic surface has also been investigated and hybrid microassembly has been demonstrated with both water and adhesive. Application relevant patterns such as segmented patterns and patterns with jagged edges have been investigated.

In summary, this thesis shows that hybrid microassembly can adapt to large varieties of patterns. Several new hybrid microassembly methods are developed and demonstrated. Such a wide adaptability and a variety of the processes indicate that hybrid microassembly can be a very promising approach for many potential applications, such as integration of surface emitting lasers, integration of small dies and 3D integration of chips with high density pin counts.

Keywords hybrid microassembly, droplet self-alignment, surface tension, self-assembly

ISBN (printed) 978-952-60-5261-8 **ISBN (pdf)** 978-952-60-5262-5

ISSN-L 1799-4934 **ISSN (printed)** 1799-4934 **ISSN (pdf)** 1799-4942

Location of publisher Espoo **Location of printing** Helsinki **Year** 2013

Pages 163 **urn** http://urn.fi/URN:ISBN:978-952-60-5262-5

Preface

The research work of this thesis was conducted in the Micro- and Nanorobotics Group at the Department of Automation and Systems Technology of Aalto University (formerly Helsinki University of Technology), Finland. I'd like to express my sincere gratitude to Prof. Quan Zhou for providing an inspiring and encouraging work environment and guiding my research through all those years. Your expertise has been of great help to me, and I have learned a lot from you ever since I first started work as a research assistant back in 2001. I would like to thank Prof. Heikki Koivo for giving me the opportunity to do my doctoral studies in his lab and for proofreading and commenting on the manuscript. I am also indebted to Dr. Tech. Veikko Sariola for valuable comments on the manuscript.

The former and current members in the Micro- and Nanorobotics Group deserve my gratitude for creating a pleasant and encouraging work environment. I warmly thank all the members I had the pleasure of working with: Veikko Sariola, Ville Liimatainen, Iiris Routa, Antti Virta, Mirva Jääskeläinen, Petri Hänninen and Petteri Korhonen.

The research work for the thesis has been carried out under several projects. I would like to thank both the Academy of Finland for funding the MUSA (2010-2013) project and the European Commission (EU) for funding the HYDROMEL (2009-2011) project, where I have worked.

I wish to thank Prof. Stephane Regnier and Prof. Marcel Tichem, who were the preliminary examiners of this thesis, for their constructive comments and suggestions which helped to improve the quality of this work.

Finally, I would like to deeply thank my parents, Mingle and Hui for their love, encouragement and continuous support throughout my life.

Espoo, March 2013
Bo Chang

List of Publications

This thesis consists of the following 10 publications.

PUB1 **Bo Chang**, Ali Shah, Iiris Routa, Harri Lipsanen, and Quan Zhou, "Surface-tension driven self-assembly of microchips on hydrophobic receptor sites with water using forced wetting," *Applied Physics Letters*, vol. 101, no. 11, p. 114105, 2012.

PUB2 **Bo Chang**, Veikko Sariola, Susanna Aura, Robin H. A. Ras, Maria Klonner, Harri Lipsanen, and Quan Zhou, "Capillary-driven self-assembly of microchips on oleophilic/oleophobic patterned surface using adhesive droplet in ambient air," *Applied Physics Letters*, vol. 99, no. 3, p. 034104, 2011.

PUB3 **Bo Chang**, Iiris Routa, Veikko Sariola, and Quan Zhou, "Self-alignment of RFID dies on four-pad patterns with water droplet for sparse self-assembly," *J. of Micromechanics and Microengineering*, vol. 21, no. 9, p. 095024, 2011.

PUB4 **Bo Chang**, Veikko Sariola, Mirva Jääskeläinen, and Quan Zhou, "Self-alignment in the stacking of microchips with mist-induced water droplets," *J. of Micromechanics and Microengineering,* vol. 21, no. 1, p. 015016, 2011.

PUB5 Ali Shah, **Bo Chang**, Sami Suihkonen, Quan Zhou, and Harri Lipsanen, "Surface-tension driven self-alignment of microchips on black silicon based hybrid template in ambient air," *J. of Microelectromechanical Systems*, vol. 22, no. 3, p. 739, 2013.

PUB6 **Bo Chang**, Antti Virta, and Quan Zhou, “Hybrid microassembly for massively parallel assembly of microchips with water mist,” in *Proc. Int. Conf. on Manipulation, Manu-facturing and Measurement on the Nanoscale*, 3M-NANO'12, September, 2012, pp. 38-43.

PUB7 **Bo Chang**, Mirva Jääskeläinen, and Quan Zhou, “Hybrid microassembly of chips on low precision patterns assisted by capillary self-alignment,” in *Proc. IEEE/RSJ Int. Conf. on Intelligent Robots and Systems*, IEEE-IROS'11, October, 2011, pp. 907–912.

PUB8 **Bo Chang**, Ville Liimatainen, Iiris Routa, and Quan Zhou, “High-accuracy positioning of microchips on patterns with jagged edges using hybrid microassembly,” in *Proc. IEEE Int. Conf. on Mechatronics and Automation*, IEEE-ICMA'12, August, 2012, pp. 807-812.

PUB9 **Bo Chang**, Mirva Jääskeläinen, and Quan Zhou, “Hybrid micro assembly of microchips on segmented patterns,” in *Proc. IEEE Int. Conf. on Automation Science and Engineering*, IEEE-CASE'10, 2010, pp. 15–20.

PUB10 **Bo Chang**, Mirva Jääskeläinen, and Quan Zhou, “Microassembly combining pick-and-place and water mist,” in *Int. Symposium on Micro-NanoMechatronics and Human Science*, MHS'10, 2010, pp. 333–337.

Contributions of the Author

All the work was under the supervision of Prof. Quan Zhou, and many initial ideas were generated based on the author's discussions with Prof. Quan Zhou.

PUB1 The author developed the concept of the forced wetting technique for hydrophobic patterns. The author wrote the article. The author designed and conducted the experiments, including setting up test platform and carrying out experiments. The numerical simulations were carried out by the author together with Ms. Iiris Routa. The author was responsible for analysis of the results. The author participated in the design and validation of the patterns used in the experiments. M.Sc. Ali Shah fabricated the patterns. Prof. Quan Zhou contributed by reviewing the article.

PUB2 The idea of using oleophilic/oleophobic patterns for adhesive self-alignment was generated by the author, Prof. Quan Zhou and Dr. Veikko Sariola. The author wrote the article together with Prof. Quan Zhou, with support of Dr. Tech. Robin Ras. The author was the primary designer and conductor of the experiments. Dr. Tech. Robin Ras developed the concept of the surface functionalization method. Dr. Tech. Veikko Sariola did microfabrication and Ms. Susanna Aura contributed the porous ORMOCER material.

PUB3 The author designed the four-pad patterns. The author conducted the experiments and wrote the main parts of the article. Ms. Iiris Routa carried out the simulations and wrote the Sections covering that in the article. Prof. Quan Zhou was the instructor of the work.

PUB4 The concept of water mist induced self-alignment was developed by the author and Prof. Quan Zhou. The author

wrote the article. The experiments and data analysis were carried out by the author with the support from M.Sc. Mirva Jääskeläinen. Dr. Veikko Sariola developed the machine vision algorithms for calibration of water mist induced droplets. Prof. Quan Zhou supervised the experiments and advised the writing of the article.

PUB5 The author carried out the experimental tests and wrote the Sections covering that in the article. Rest of the article was written by M.Sc. Ali Shah.

PUB6 The idea of parallel assembly of microchips using water mist was generated by the author and Prof. Quan Zhou. The author wrote the article. The author developed the test platform and conducted the experiments. The author inspected the alignment accuracy using environmental scanning electron microscope (ESEM) with support from Mr. Antti Virta. Prof. Quan Zhou supervised the experiments.

PUB7 The author designed the low-precision patterns together with M.Sc. Mirva Jääskeläinen. The author wrote the article. The experiments were carried out by the author and M.Sc. Mirva Jääskeläinen. The author analyzed the results. Prof. Quan Zhou contributed by reviewing the article.

PUB8 The author wrote the article. The author developed the algorithm for measurement of positioning accuracy. The patterns used in the experiments were designed by the author and Ms. Iiris Routa. M.Sc. Ville Liimatainen fabricated the patterns. Prof. Quan Zhou commented on the manuscript.

PUB9 The author wrote the article. The author designed the patterns and carried out the experimental work with M.Sc. Mirva Jääskeläinen. Prof. Quan Zhou reviewed the article.

PUB10 The author wrote the article. The experiments were performed by the author together with M.Sc. Mirva Jääskeläinen. The author was responsible for the data analysis. Prof. Quan Zhou supervised the experiments.

Symbols

Symbol	Unit	Definition
A	m^2	Surface area of the liquid interface
E	J	Surface energy
f		Fraction of solid surface area wet by the liquid, $0 \leq f \leq 1$
F	N	Restoring force
g	m/s^2	Gravitational acceleration
G	J	Gibbs free energy
G_f	N	Gravitational force
h	m	Liquid droplet film thickness
L	m	Part length
m	kg	Part mass
p_C	Pa	Characteristic pressure of liquid
R	m	Principal radii of curvature
R'	m	Principal radii of curvature
T	Nm	Torque
V	m^3	Volume of chip
w	m	Part width
W	J	Mechanical work
x	m	x-bias, the difference between the initial position and the equilibrium position of a part during self-alignment
y	m	y-bias, the difference between the initial position and the equilibrium position of a part during self-alignment
z	m	z-bias, the difference between the initial position and the equilibrium position of a part during self-alignment

Symbol	Unit	Definition
α	o	Pad edge angle
γ	J/m²	Surface energy. For liquids equal to surface tension.
γ_{SL} , γ_{LG} , γ_{SG}	J/m²	Surface energies of the solid-liquid, liquid-gas and solid-gas interfaces, respectively
Δp	Pa	Overpressure inside a meniscus
θ	o	Contact angle on the sharp edge
θ_A	o	Apparent Contact angle
θ_C	o	Young's contact angle
λ_c	m	Capillary length of liquid
ρ	kg/m³	Liquid density

Abbreviations

CA	Contact angle
ESEM	Environmental scanning electron microscopy
RFID	Radio-frequency identification
RIE	Reactive-ion etching
SEM	Scanning electron microscope
SiO_2	Silicon dioxide
STD	Standard deviation
SU-8	A negative, high aspect-ratio photoresist
TCL	Three-phase contact line
VCSEL	Vertical-carity surface-emitting laser

Contents

Preface i

List of Publications iii

Contributions of the Author v

Symbols vii

Abbreviations ix

Contents xi

1. Introduction 1

1.1 Background 1

1.2 Motivation and objectives 3

1.3 Contributions 4

1.4 Summaries of the publications 5

1.5 Structure of the thesis 6

2. Foundation of Surface Tension Driven Droplet Self-alignment 7

2.1 Surface tension 7

2.2 Wetting and contact angle 8

2.2.1 Wetting on ideal surface 8

2.2.2 Wetting on patterned surface 10

2.2.3 Wetting on planar patterns 12

2.3 Surface tension driven droplet self-alignment 13

3. Hybrid Microassembly Handling Strategies 17

3.1 Droplet assisted hybrid microassembly 17

3.2 Water mist induced hybrid microassembly 18

3.3 Hybrid microassembly with forced wetting 20

4. Patterns for Hybrid Microassembly 23

4.1 Oleophilic/ oleophobic nano-structured surface..... 23

4.1.1 Porous ormocer functionalized with fluorinated trichlorosilane 23

4.1.2 Black silicon coated with fluoropolymer 24

4.2 Hydrophilic/hydrophobic micro-patterned surface 26

4.2.1 Segmented patterns 26

4.2.2 Patterns with jagged edges 28

4.3 Patterns with geometric solid edges 30

5. Results and Discussions 31

5.1 Experimental set-up 31

5.2 Self-alignment on hydrophobic patterns (PUB1)..... 32

5.3 Self-alignment using adhesive in air (PUB2, 5)..... 33

5.4 Self-alignment on segmented patterns (PUB3, P9) 36

5.5 Self-alignment with water mist (PUB4, 6, 10) 38

5.6 Self-alignment on patterns with jagged edges (PUB7, 8) 42

6. Conclusions 45

References 49

Appendix: Publications..... 55

1. Introduction

This section briefly introduces the background of the thesis and summarizes the contributions.

1.1 Background

Assembly refers to "the fitting together of manufactured parts into a complete machine, structure, or unit of a machine" according to Merriam-Webster On-line Dictionary. **Microassembly** commonly refers to assembly of micro parts, i.e. parts of which one or more dimensions are less than 1 mm [1]. Microassembly is a rapidly emerging and groundbreaking technology to build highly integrated micro- and nanosystems. One of the most important assembly steps is the precise positioning of the micro parts, which normally requires the alignment of micro objects with features such as edges or surface structures. The major challenge in microassembly is not only the reduced size, but also the **scaling effect** [2]. Adhesion forces, such as van der Waals forces, electrostatic forces and capillary forces, become more dominant than inertial and gravity forces between the tiny components. This causes serious problems in microassembly, e.g. unwanted adhesion between parts and tools which consequently affect the precision and efficiency of the assembly [3].

Many techniques have been developed to tackle the problems in microassembly. Those techniques can be categorized mainly in three areas. The first one is **robotic pick-and-place** based assembly approach. This technique is usually based on one or several micromanipulation systems, having tools such as a microgripper, a micro positioning system, a vision system, and a control system. To achieve assembly, a bonding or a fixing tool is also needed. The development of robotic pick-and-place system started in 1990s and many prototypes have been developed [4–8]. The robotic pick-and-place approach has been extensively pursued due to its flexibility and good adaptability. Currently, microassembly is carried out in industry using e.g. an automatic flip chip machine aided by machine vision and it can achieve high throughput up to 10,000 units per hour at a relatively good

accuracy of 6μm [9]. However, the assembly towards smaller chips (e.g. 100 μm lateral dimensions) requires much higher alignment accuracy, e.g. around 1 μm. Even though such a requirement can be achieved using the traditional robotic technology, the throughput is severely reduced (e.g. 240 units per hour for 0.5μm accuracy [10]). Furthermore, for robotic pick-and-place, the final positioning of the object is determined by the manipulation status before releasing. Without properly designed fixing strategy (e.g. form-closure, bonding, adhesive), the placing process can be very tedious and time-costly due to the adhesion between the tool and the object. To enable easy releasing, it is usually suggested that the end-effector of the tools has a rough surface and is conductive and grounded [11][12][13]. Various manipulation strategies have also been proposed, e.g. pick-and-place strategy using a rod [14] or a high-frequency vibration release [15]. Despite all those efforts spanning the past ten plus years, the problem remains a major challenging issue with robotic pick-and-place based assembly approach.

The second microassembly approach is **self-assembly**, which is based on the principle of minimum potential energy, where the gradient of potential is designed to drive the parts toward desired locations. Different self-assembly techniques for placing microchips have been proposed based on e.g. geometrical shape recognition and gravity [16] or surface patterns and capillary forces [17–24], where the processes are carried out in a fluidic bath. Some of the self-assembly processes have also been carried out in air, using different physical principles such as electric field [25], magnetic field [26] or geometric shape recognition [27–31]. Those self-assembly techniques have claimed impressive results, e.g. 62500 chips assembled in 45 seconds [24]. Self-assembly technology can also reach very good precision, e.g. sub-micron range [24]. By careful design, using techniques such as multi-phase self-assembly [32] [33] and surface tension based self-folding ([34], [35], [36]), relatively complicated microstructures and even 3D microsystem can be implemented. The advantage of a self-assembly technique is that the final positioning of the objects is automatic (by design) which makes massive parallel operation possible. However, the processes developed so far are aiming mainly at mass production of simple micro structures. Even though it is possible to use multi-batch process to extend the complicity of the target structure, it is not competitive with the flexibility and dexterities of robotic pick-and-place approach.

To tackle the challenge of achieving good flexibility and high efficiency simultaneously, a third microassembly technique has been proposed recently. The technique is the so-called **hybrid microassembly** technology [37], [38], which combines self-assembly technology with traditional robotic

pick-and-place technology or other robotic feeding mechanics to construct microsystems flexibly. In those hybrid microassembly studies [39–41], a micro part is brought adjacent to the assembly site by a robot handling tool at a high speed but with a relatively low precision, and water droplets dispensed by a dispenser at the assembly site align the part at a higher precision. The study [39] evaluated the yield, accuracy, capability and speed of hybrid microassembly. The results have shown that hybrid assembly technique can achieve more deterministic results and new constructions that are not possible with self-assembly alone simultaneously. It gives high-yield (99%) and high-precision (sub-micrometer) that is not possible using robotic pick-and-place approach. The speed of the hybrid microassembly mainly depends on the speed of the robotic handling tool. In a recent industrial demonstration of hybrid microassembly, a throughput of over 40,000 unit has been reported [42]. In the demonstration, the dies were placed by a robotic pick-and-place tool at the speed of over 40,000 unit per hour, and the surface tension driven self-alignment occurred subsequently after the placement. Because the cycle time of robotic pick-and-place (less than 90 ms) may be shorter than the self-alignment duration, the surface-tension driven self-alignment continued acting while the sub sequential robot actions were carried out. Micron accuracy positioning was achieved in final positioning.

1.2 Motivation and objectives

Hybrid microassembly solves the problem of trade-off between robotic pick-and-place and self-assembly technique. However, it is largely an open question how well the hybrid microassembly is adaptable to large variety of micro parts and the corresponding patterns in the potential real-world applications. In the RFID tag assembly or other low-pin count package assembly, it is very common that there are several electrical contacts (bumps) on the chips, and the pattern normally consists of segmented structures corresponding to the electrical contacts on the chips. Micro parts and patterns often contains defects on their edges due to the imperfection in low-cost manufacturing process. Furthermore, the patterns can be hydrophobic or hydrophilic, planar or protruded with sharp solid edges. In this thesis, experimental investigations were carried out using different types of planar patterns including segmented patterns, patterns with defects, hydrophilic patterns, hydrophobic patterns, as well as patterns with sharp solid edges. The first goal was to investigate what kind of patterns are suitable for hybrid microassembly.

In the previous hybrid microassembly studies, water droplet have been used as the media for alignment in hybrid microassembly. Use of a water droplet is a simple and efficient way to achieve fast-speed and high-precision alignment. There are, however, also some limitations: 1) a water droplet cannot provide permanent bonding; 2) a water droplet is dispensed on the pattern one by one, and therefore parallel assembly is not possible; 3) extra fabrication steps are needed for fabricating hydrophilic patterns and hydrophobic substrate. This is the preferable way for water droplet self-alignment in the air. These limitations hinder the effectiveness of hybrid microassembly in practical applications. Therefore, the second goal of this thesis is to develop different hybrid microassembly approaches which can meet the specific needs in potential applications and relax the fabrication requirement for patterns.

1.3 Contributions

Firstly, this thesis brings new knowledge about patterns suitable for hybrid microassembly. Four different types of patterns have been investigated, and they include (1) segmented patterns, (2) patterns with jagged edges, (3) oleophilic/phobic patterns and (4) hybrid template. The contributions are listed based on the type of the patterns used as follows:

(1) *Segmented patterns:* Self-alignment of microchips has been demonstrated on segmented patterns. The influence of the key parameters affecting the self-alignment on segmented patterns has been studied both theoretically and experimentally.
(2) *Patterns with jagged edges*: Self-alignment of microchips has been demonstrated on patterns with jagged edges. Experiments have been carried out to study the effect of patterns with jagged edges on self-alignment.
(3) *Oleophilic/phobic patterns*: First demonstration of a patterned oleophilic/oleophobic surface for self-alignment of microchips using an adhesive droplet in ambient air environment.
(4) *Hybrid template*: Self-alignment of microchips on a simple-to-fabricate hybrid template has been demonstrated with both water and adhesive.

Secondly, this thesis provides experimental evidence and theoretical analysis for evaluation of three different hybrid microassembly handling strategies: (1) droplet assisted hybrid microassembly, (2) water mist induced hybrid

microassembly, (3) hybrid microassembly with forced wetting. The contributions are classified based on the method:

(1) *Droplet assisted hybrid microassembly*: The droplet self-alignment has been demonstrated on patterns with segments and patterns with jagged edges.
(2) *Water mist induced hybrid microassembly*: Parallel self-alignment of microchips with water mist induced hybrid microassembly has been demonstrated for the first time. Investigation has been carried out to understand the physics of the accumulation process of water mist.
(3) *Hybrid microassembly with forced wetting*: Self-alignment on hydrophobic pattern with super-hydrophobic substrate has been demonstrated using hybrid microassembly with two forced wetting techniques: a) introducing excessive amount of water; b) applying external pressure to force the water to wet the hydrophobic patterns.

1.4 Summaries of the publications

This thesis consists of ten publications, which were published during the years 2010-2013. The publications include studies of the hybrid microassembly technique using different handling strategies and patterns. **PUB1** reports self-alignment of microchips on hydrophobic patterns with super-hydrophobic substrate using forced wetting, by either introducing an excessive amount of water or applying external pressure to force the water to wet the hydrophobic patterns. **PUB2** reports the first demonstration of a patterned oleophilic/oleophobic surface for self-alignment of microchips using an adhesive droplet in ambient air environment. **PUB3** investigates the influences of the key parameters, such as the volume of the droplet, the gaps between the pads and the initial bias that may affect the self-alignment on segmented patterns both theoretically and experimentally. **PUB4** reports the in-depth study of water mist induced hybrid microassembly and investigates the physics of the accumulation process of water mist. **PUB5** reports the fabrication and use of a hybrid black silicon template for self-alignment of microchips with water or adhesive. **PUB6** reports the first demonstration of water mist induced hybrid microassembly technique used for massively parallel assembly of microchips. **PUB7** investigates the effect of low precision patterns on self-alignment of RFID chips. Special segmented patterns having jagged edges have been purposely designed and fabricated to mimic some real-world RFID antennas. **PUB8** reports about the positioning accuracy of microchips on patterns with regular edge jaggedness

as well as with random edge jaggedness using droplet assisted hybrid microassembly technique. **PUB9** reports about a novel process of a droplet assisted hybrid microassembly technique for assembly of RFID chips on segmented patterns. **PUB10** proposed a water mist induced hybrid microassembly technique for self-alignment of microchips.

1.5 Structure of the thesis

The thesis is organized as follows. Chapter 2 introduces the foundation of droplet self-alignment through surface tension, wetting phenomenon and contact angles. Chapter 3 presents different hybrid microassembly handling strategies in order to combine the traditional robotic pick-and-place technique with the self-alignment technique. Various patterns used for hybrid microassembly are introduced in Chapter 4. Chapter 5 summarizes and discusses the main results of the thesis. Finally conclusions are drawn in Chapter 6.

2. Foundation of Surface Tension Driven Droplet Self-alignment

The droplet self-alignment process discussed in this thesis is driven by surface tension. This section introduces the physical origins of the surface tension and wetting.

2.1 Surface tension

Droplet self-alignment is driven by surface tension, which can be explained at the molecular level and defined on a macroscopic scale. At molecular level (**Fig.1**), a liquid molecule in the middle of the liquid is pulled in all directions equally by neighboring liquid molecules, resulting in a net force of zero. On the other hand, a liquid molecule close to the surface does not have other liquid molecules on all sides. Therefore it is pulled inwards in the liquid, where internal pressure is built up around it. This forces the surface of liquid to contract to a minimal area. The surface tension can be also explained in terms of energy. A molecule is in a lower state of energy when it is in contact with a neighboring molecule than if it were alone. The molecules inside the liquid have as many neighbors as they can possibly have, but the molecules closes to the surface are missing liquid neighbors and therefore have a higher energy level. For the liquid to minimize its energy state, the number of higher energy molecules must be minimized.

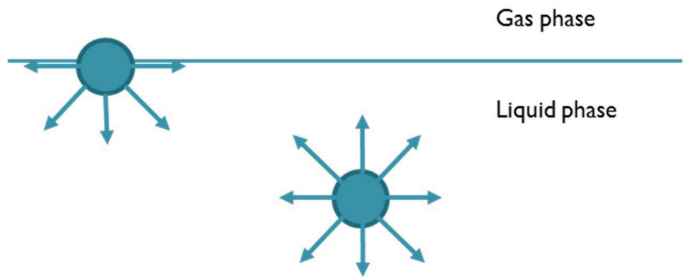

Fig.1 A molecule stationed at the surface is missing half of intermolecular attractions.

On a macroscopic scale, surface tension represented by the symbol γ can be defined as the force along a line of unit length which the force acts or as the

work must be done to increase surface area by one unit. Therefore, the surface tension can be expressed as $\gamma = \frac{F}{L}$ (Nm^{-1}) or $\gamma = \frac{\delta W}{\delta A}$ (Jm^{-2}), where F is the force, L the length, A is the surface area and W is the mechanical work. In thermodynamics, surface tension can be defined as the increase in internal energy or Gibbs free energy per surface area, which can be expressed as $\gamma = \frac{\delta G}{\delta A}$, where G is Gibbs free energy. Thermodynamics requires that all spontaneous changes of state are accompanied by a decrease in Gibbs free energy. This explains why the liquid decreases its surface area spontaneously as the Gibbs free energy decreases. When a liquid reaches its equilibrium state, minimum surface area satisfies the Young-Laplace equation, which relates the overpressure existing in the interior of the drops to the shape of the surface.

$$\Delta p = \gamma\left(\frac{1}{R} + \frac{1}{R'}\right) \tag{1}$$

where R and R' are the radii of the curvature of the surface, Δp is the pressure difference.

2.2 Wetting and contact angle

Wetting plays a very important role in droplet self-alignment because alignment requires good wetting and confinement of droplet on the desired area. Wetting refers to the ability of a liquid to maintain contact with a solid surface, resulting from intermolecular interactions when the two are brought together. Adhesive forces between a liquid and solid cause a liquid droplet to spread. Cohesive forces within the liquid cause the droplet to ball up and avoid contact with the surface. The wettability is determined by the balance between the adhesive and cohesive forces. The contact angle that a liquid droplet forms over a surface is a measure of the tendency of the liquid to wet the solid, and it is determined by the balance of the solid-gas, solid-liquid and liquid-gas surface tensions at the interface. As the tendency of a droplet to spread out over a flat, solid surface increases, the contact angle decreases. Thus, the contact angle provides an inverse measure of wettability.

2.2.1 Wetting on ideal surface

An ideal solid surface is one that is flat, rigid, perfectly smooth, chemically homogeneous, and has zero contact angle hysteresis. Zero hysteresis implies

that the advancing and receding contact angles are equal. In other words, there is only one thermodynamically stable contact angle. When the surface is flat and homogenous, the contact angle (CA) θ_C of a liquid droplet shown in **Fig.2** can be calculated based on Young's equation[43]:

$$\cos\theta_c = \frac{\gamma_{SG} + \gamma_{SL}}{\gamma_{LG}} \tag{2}$$

where γ_{SG}, γ_{SL} and γ_{LG} are the surface tensions between the three phases: solid-gas, solid-liquid and liquid-gas respectively. The region where three immiscible coexisting phases meet is called the three-phase contact line (TCL).

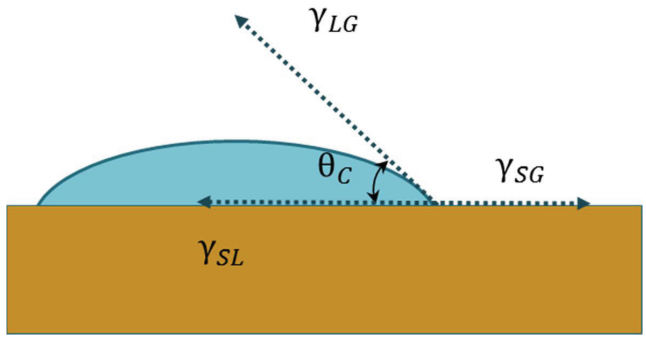

Fig.2 A liquid droplet rests on a solid surface and is surrounded by gas. The contact angle θ_C is the angle formed by a liquid at the three phase boundary where the liquid, gas, and solid intersect.

There are two types of surfaces the liquid can interact, which includes a high-energy surface and a low-energy surface. The material with high surface energy exhibits a small contact angle, whereas the surface with low surface energy shows a high contact angle.

Surface with poor wettability can be realized by coating it with low surface energy materials, such as Teflon like polymer. However, low surface tension liquid, such as oil, has a very good wetting property on most of the surfaces including the surface coated with low surface tension material. Compared to the surface with poor wettability, the surface with good wettability is rather easy to find in nature. For example, most liquids achieve good wetting with high energy surface, such as metals, glass and ceramics. A super hydrophobic surface or oleophobic surface can be realized using a combination of the low surface energy coating and nano topographical structures. More details are given in the next section.

2.2.2 Wetting on patterned surface

When the surface is non-homogenous and contains roughness, it becomes inhomogeneous and the Young's equation cannot be directly applied in this situation. Two other models are normally used to explain the wetting behavior, namely Wenzel [44] or Cassie-Baxter models [45]. Based on these models the droplet characteristics are shown in **Fig.3**. The droplet can either penetrate into the roughness (**Fig.3** (a)) or it can pin on top of the structures forming a higher contact angle (**Fig.3** (b)). On an intrinsically hydrophilic surface, the introduction of roughness leads to an increase in hydrophilicity, whereas, on hydrophobic surface the roughness increases hydrophobicity and the droplet usually takes up the Cassie-Baxter state [45]. As shown in **Fig.3** (b), in Cassie-Baxter state, the droplet assumes that the air pockets are trapped underneath the liquid droplet in a way that the peaks of roughness features are in contact with the liquid droplet. The apparent contact angle θ_A is given by:

$$\cos\theta_A = f(\cos\theta_c + 1) - 1 \tag{3}$$

where f is the areal fraction of the solid surface in contact with the liquid droplet and θ_C is the Young's contact angle on the smooth surface.

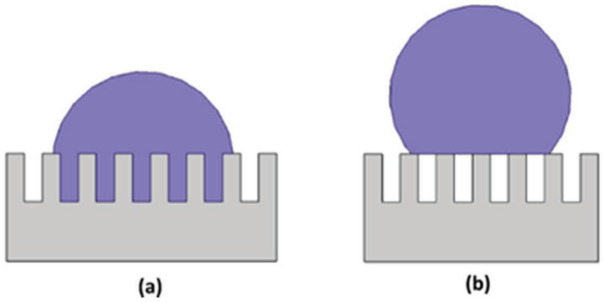

Fig.3 Liquid droplet behavior on rough surface: (a) Wenzel state (b) Cassie- Baxter state.

Cassie–Baxter model has been widely applied to predict the apparent contact angles obtained on heterogeneous surfaces. However, validity of the Cassie-Baxter model has been heavily questioned by various groups. Gao and McCarthy [46] have challenged the validity of the model by demonstrating significant differences between the model predictions and their experimental measurements of the apparent contact angles on heterogeneous surfaces. Various groups such as [46], [47] and [48] have claimed that the apparent contact angle is determined by the linear fractions of solid and air calculated along the three-phase contact line, not by the overall areal fractions. Despite

the limitation of the Cassie-Baxter model, it can be used to explain the hydrophobicity of surface with roughness, which is sufficient for this thesis.

In this thesis, another kind of patterned surface refers to the surface with patterns having geometric solid edges. The edges can be used as a boundary for liquid confinement. The droplets are first dispensed on top of the pattern. Then the liquid front proceeds towards the edges. The behavior of the advancing droplet on solid edges can be described with Gibbs' inequality:

$$\theta_C \le \theta \le (180° - \alpha) + \theta_C \tag{4}$$

where θ is the droplet contact angle on the edge, θ_C is the Young's contact angle and α is the edge angle. Based on Gibbs condition and the schematic in **Fig.4**, the edges with smaller α values, have proven to be able to confine larger amounts of liquid within the target area, before the liquid front is able to cross the solid edge.

As shown in **Fig.4**, the contact angle θ may extend over a range of angles based on (4). Studies conducted in [49] assume that the upper limit of θ on the edge that a droplet can attain can be written as:

$$\theta = (180° - \alpha) + \theta_C \tag{5}$$

Once the droplet reaches θ_C, the possibility whether the droplet will keep the contact line or it will tumble along the protrusion is related to α [49]. At smaller scales, when the effect of gravity is negligible, if $\alpha \leqslant \theta_C$ then $\theta \geqslant 180°$. The droplet protrusion stays confined to a point where the effect of gravity is appreciable. After that, it will cross the edge and roll over the protrusion. On the other hand, if $\alpha \geqslant \theta_C$ so that $\theta \leqslant 180°$, the increase in the droplet volume after droplet reaches θ_C will cause the droplet to move over the edge or its sudden spreading down the protrusion.

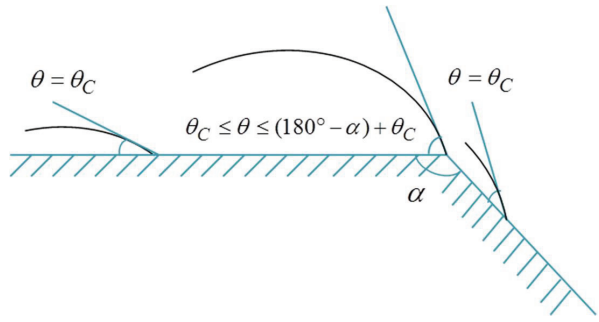

Fig.4 Droplet contact angle on the solid edge.

There are different alternatives (**Fig.5**) for creating solid edges on the surface, e.g. protruding patterns and trenched patterns. Recently, it has been demonstrated that the undercut edge can also prohibit liquid from spreading [50].

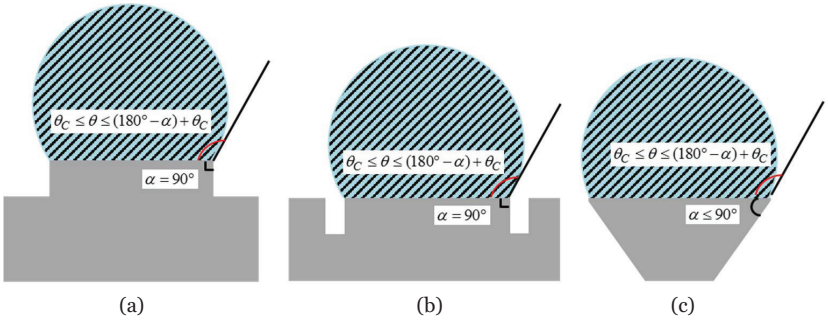

Fig.5 Alternatives of solid edges on the surface: (a) protruding pattern, (b) trenched pattern, (c) pattern with undercut edge.

2.2.3 Wetting on planar patterns

Planar patterns refer to the surface consisting of planar patterns on substrate. The patterns and the substrate are normally made of different materials and therefore have different wettability. The wetting contrast between the patterns and substrate can be used to create a boundary for liquid confinement. The general rule for designing the pattern and the substrate for droplet self-alignment is that the pattern should be lyophilic (against the lyophobic background) to the liquid medium between the pattern and the microchip to be assembled. An example is a hydrophilic pattern, if water is used as the self-assembly medium in the air as shown in **Fig.6** (a). Here the water droplet is prevented spreading from a hydrophilic area to hydrophobic substrate in the air. **Fig.6** (b) shows that the adhesive droplet is confined inside a hydrophobic but oleophilic area with hydrophilic background in water.

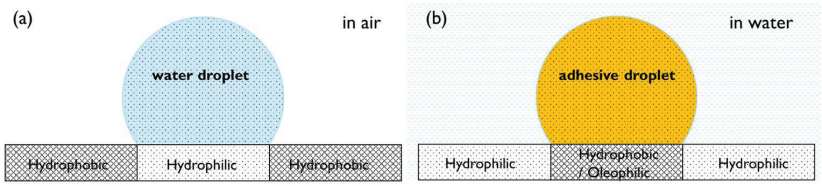

Fig.6 (a) a water droplet is confined within a hydrophilic pattern with hydrophobic substrate in air; (b) an adhesive droplet is confined within a hydrophobic but oleophilic pattern with hydrophilic substrate in water.

The poor wettability of the surface can be normally achieved by low surface energy fluoropolymer coating. Because the low surface energy fluoropolymer coating changes the chemical composition of the surface [51], it makes hard for the water droplet to spread on the surface and therefore the droplet exhibits high contact angle.

2.3 Surface tension driven droplet self-alignment

In surface tension driven droplet self-alignment prcocess, a droplet of a liquid is placed between a chip and a matching pattern, the droplet forms a meniscus and aligns the chip to the pattern. This thesis uses the term *droplet self-alignment* to represent *surface tension driven droplet self-alignment* for simplicity. The term *bias* is defined as the difference between the initial position and the equilibrium position of a chip after self-alignment. Droplet self-alignment uses the principle of minimum surface energy of the liquid droplet, where the gradient of potential drives the parts toward the desired alignment locations. A liquid droplet is in a stable equilibrium, when its surface energy is at a minimum. In turn, the surface energy is at a minimum when the surface area is minimal. The restoring force is the force that drives a liquid menisucs to a position where its surface energy is at a minimum. To calculate the surface energy and restoring forces in droplet self-alignment, the shape of the liquid meniscus can be approximated with planar surfaces, as shown in **Fig.7**.

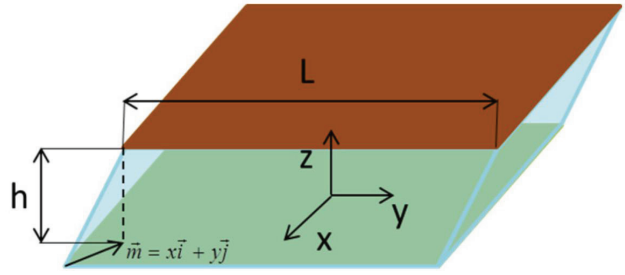

Fig.7 Approximation of the liquid meniscus between a part and a pattern with the translational biases.

When gravity of the liquid droplet is not considered in the simulation, the results are applicable only at the scale smaller than the capillary length. The capillary length for clean water at standard temperature and pressure is about 2.7mm. When the initial placement error or biases are introduced, the restoring force acting on the chip and directing the meniscus to the desired position can be calculated by:

$$\vec{E}(x,y) = -\nabla E(x,y) = -\nabla(\gamma A(x,y)) \tag{6}$$

where E is the surface energy of the liquid meniscus, γ is the surface tension and A is the area of the surface between liquid and air. The surface energy of the liquid meniscus is approximated as:

$$E_{ref}(x,y) = \gamma A(x,y) = 2\gamma L(\sqrt{x^2+y^2} + \sqrt{y^2+h^2}) \tag{7}$$

where x and y are the biases along the corresponding axes, L is the length of the pattern and the chip, h is the height of the liquid meniscus. Using (7), the base model for restoring force becomes

$$\vec{F}_{ref}(x,y) = -2\gamma L(\frac{x}{\sqrt{x^2+h^2}}\vec{i} + \frac{y}{\sqrt{y^2+h^2}}\vec{j}) \tag{8}$$

As the surface shape of the liquid in reality is curved, a more accurate numerical model can be created using program 'Surface Evolver' [52]. It finds the (quasi) static equilibrium for liquid medium by evolving the surface using the gradient descent method. The software breaks the surface of the object into smaller elements, and tries to minimize the surface energy of each element, by optimizing the location of each vertex. It uses gradient descent method for moving the vertexes.

Fig.8 shows one example of numerical simulation of the droplet self-alignment using 'Surface Evolver', where three elements are used: a chip, a droplet of water and a pattern on the substrate. In this particular simulation, the contact angle of the pattern and the substrate is first 30° and then 180°. The volume of the droplet is 0.9 nanolitres (nL), and the reason for choosing this amount of water droplet is that it is sufficient to wet the bottom of the chip and the surface of the pattern.

As shown in **Fig.8** (a)-(d), a chip is released above a pattern where a droplet of water lies, and a meniscus is formed between the chip and the pattern (**Fig.8** (a)). The shape of the meniscus generates a so-called restoring force that moves the chip towards the pattern to minimize the total surface energy of the meniscus (**Fig.8** (b)-(c)). Finally, the chip stops at the location where the surface energy of meniscus is minimized and the water evaporates (**Fig.8** (d)).

Fig.8 (e)-(f) shows the relation between the energy and the restoring force with respect to bias in x-axis. Both energy and restoring force curves indicate that the water meniscus reaches its equilibrium state when the bias in x-axis

becomes zero. Therefore, the chip keeps moving until the misalignment disappears.

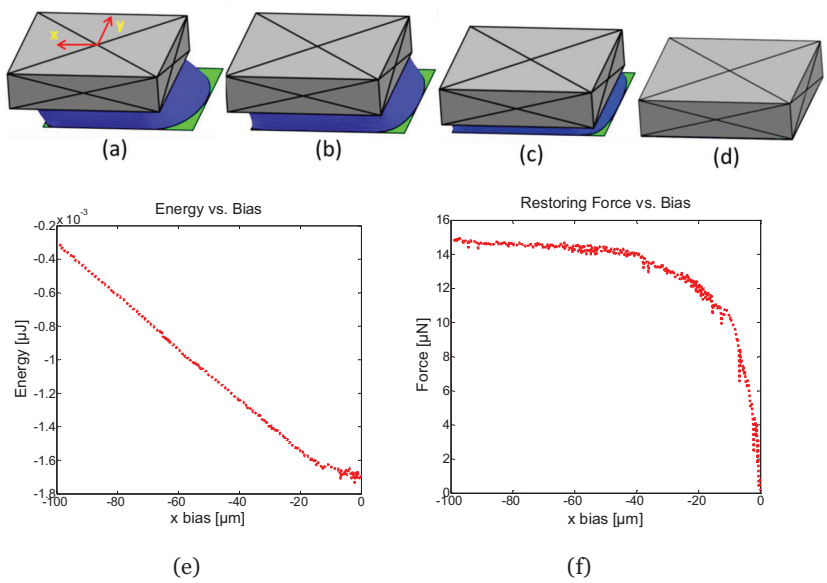

Fig.8 Numerical simulation of water droplet self-alignment of a microchip on a hydrophilic pattern with volume of water: 0.9 *nL*, size of chip and pattern: 200μm × 200μm and water contact angle of pattern, substrate and chip: 30°/180°/80° respectively. (a) a chip is above a pattern with a droplet of water in middle; (b) and (c) the droplet minimizes its surface area and moves the chip towards the pattern; and finally water evaporates and alignment is achieved in (d). (e) Energy curve and (f) restoring force curve of water meniscus with respect of x-bias.

In the droplet self-alignment numerical simulation, the gravitational force acting on the chip is neglected because the size of the chip (200μm×200μm×50μm) is very small. To demonstrate that the gravitational force is significantly smaller than the restoring force, the gravitational force of a 200μm×200μm×50μm SU-8 chip has been compared with the restoring force of 0.9 *nL* water for self-alignment. The gravitational force of a 200μm × 200μm × 50μm SU-8 chip can be calculated from

$$G_f = mg = d \cdot V \cdot g \tag{9}$$

where m is the mass of the chip, g is the gravitational acceleration with an average magnitude of 9.81 m/s^2, d is the density of SU-8 2025 (1.219g/ml or 1.219*103kg/m^3 based on datasheet from MICROCHEM), V is the volume of the SU-8 chip. Therefore, the gravitational force of the chip is:

$$G = mg = 2.438 \times 10^{-9} kg \times 9.8 N/kg = 2.39 \times 10^{-8} N = 0.0239 \mu N \quad (10)$$

The restoring force acting on the chip consists of lateral and vertical force. At a later phase of self-alignment process, the volume of the water decreases as it evaporates. To compare the gravitational force with the restoring force during evaporation of water, the Surface Evolver is used to simulate both the lateral (in x-axis) and vertical restoring force (in z-axis) with different volume of water: 0.9, 0.5 and 0.2 *nL*. The results are shown in **Fig.9** (a) indicating that the restoring force in x-axis is significantly larger than the gravitational force (0.0239μN) of the chip.

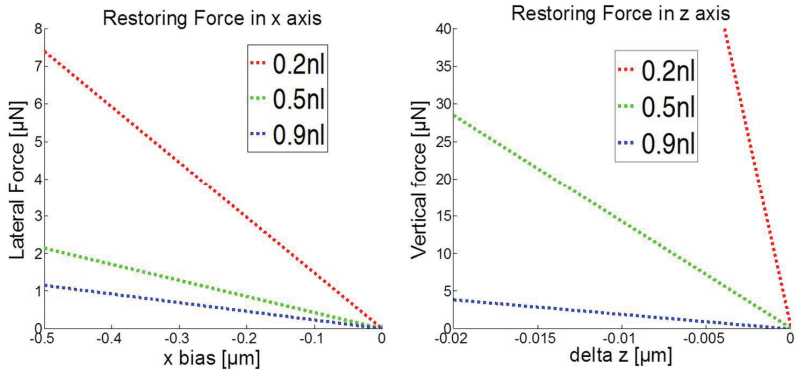

(a) (b)

Fig.9 Numerical simulation of restoring force acting on a microchip with volume of water: 0.9 *nL*, 0.5 *nL* and 0.2 *nL*, size of the chip: 200μm × 200μm × 50μm. (a) Lateral restoring force with respect to the x bias; (b) Vertical restoring force with respect to the delta z (difference between the equilibrium position and height of the liquid meniscus).

Fig.9 (b) shows the vertical restoring force with respect to the delta z (difference between the equilibrium position and height of the liquid meniscus). When the volume of water is 0.2 *nL*, the red curve in **Fig.9** (b) shows that the restoring force acting in z-axis is about 7200μN/μm, which means the gravitational force (0.0239μN) can cause the displacement in z-axis equivalent to 3.3×10^{-3}nm. This is extremely small and should be neglected.

In conclusion, the gravitational force acting on a SU-8 chip with size of 200μm × 200μm × 50μm is significantly smaller than the lateral and vertical restoring force acting on the chip. Therefore, the gravitational force can be neglected during the self-alignment process.

3. Hybrid Microassembly Handling Strategies

Hybrid microassembly combines the traditional robotic pick-and-place technique with the droplet self-alignment technique. This technique utilizes the fast-speed robotic handling tool for the coarse positioning and applies the droplet self-alignment technique to achieve high-accuracy alignment. Hybrid microassembly takes advantages of both robotic assembly technique and the droplet self-alignment technique. In this section, different handling strategies are investigated and new strategies are proposed. The handling strategies are grouped into three categories: **droplet assisted hybrid microassembly**, **water mist induced hybrid microassembly** and **hybrid microassembly with forced wetting**.

3.1 Droplet assisted hybrid microassembly

The typical droplet assisted hybrid microassembly procedure consists of initial robotic positioning followed by droplet self-alignment steps, shown in **Fig.10** (a)-(f).

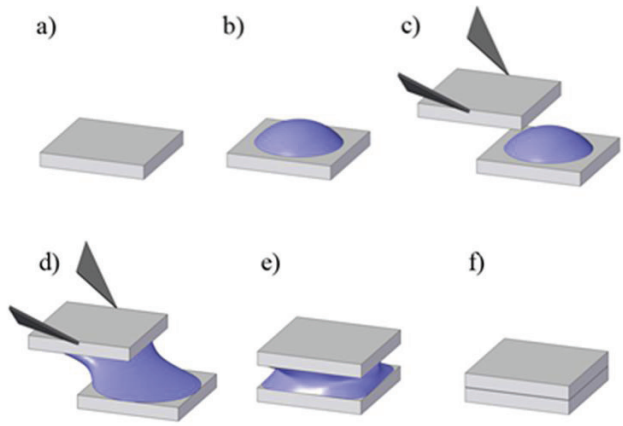

Fig.10 Droplet assisted hybrid microassembly procedure: (a) a pattern is placed at the site for assembly; (b) a droplet of liquid is dispensed on the pattern; (c) a microchip is moved towards the pattern; (d) the microchip is released from a micro handling tool and liquid wets the pattern and the bottom of the chip; (e) the chip is self-aligned with pattern due to minimum surface energy; (f) final bonding is created.

Bonding can be achieved by the process of evaporation, curing or thermal compression depending on what kind of liquid and pattern materials are applied. Releasing of the microchip is normally difficult in microassembly due to scaling laws in the micro world. When the dimensions of the elements decrease from the macroscopic to the micrometer size, the effects of gravity and inertia become negligible compared with adhesive and friction. As the surface tension of the droplet dominates the gravity during microassembly process as demonstrated in Section 2.3, the surface tension can drive the chip to align with the pattern and prevent the chip from sticking to the micro handling tool.

The patterns for assembly can be either flat or protruded. The shape of the pattern should match the microchip to be assembled. The key factor in determination of success or failure in droplet self-alignment is whether the liquid droplet is confined within the edges of the pattern during the process. The confinement of the liquid droplet can be achieved on flat patterns through large wetting contrast or on protruded patterns with geometrically solid edges. In the case of flat patterns, the substrate should be lyophobic and the pattern lyophilic with respect to the liquid medium used for self-alignment. For protruded patterns, geometric solid edges can be used as boundary to prevent the droplet spreading outside the pattern. The principle of the droplet confinement is explained in Chapter 2. More details about the design process and fabrication of the patterns are discussed in Chapter 4.

3.2 Water mist induced hybrid microassembly

The concept of water mist induced hybrid microassembly is similar to droplet assisted hybrid microassembly. However, it uses water mist instead of a single droplet to assist the robotic handling tool for microassembly. Water mist is a cloud of small water droplets suspended in the air. Once they fall onto the surface, many small droplets will form on it. Water mist, as a medium for microassembly, has several interesting properties. It can generate a massive amount of small droplets in the range of microns, which allows applications in smaller microchips, e.g. less than 100 μm in lateral dimension. These small droplets are difficult to generate in mass using precision dispensers. The volume of the water droplets can be easily controlled by regulating the power of the generator and the duration of the operation. It also allows the self-alignment process to be carried out in a normal air environment, which is favorable in many applications. Furthermore, water mist can be applied to parallel microassembly.

To investigate the water mist induced hybrid microassembly, two different approaches of microassembly are studied. In the first approach, so-called water mist-first approach, water mist is introduced first, then the chip is released from the micro handling tool, and placed on top of the pattern. In the second approach, so-called water mist-last approach, the chip is first released from the micro handling tool, then placed on top of the pattern, and finally water mist is added for precise alignment. These two approaches are shown in **Fig.11 (**a)-(b). Water mist can also be applied for parallel self-alignment as shown in **Fig.11(**c)-(e). The microchips are first roughly placed on top of a matrix of patterns fixed on the substrate with placement errors using fast robotic handling tool. Then water droplets are delivered to the assembly site in the form of water mist. Finally, all the microchips are aligned with the corresponding pattern in parallel.

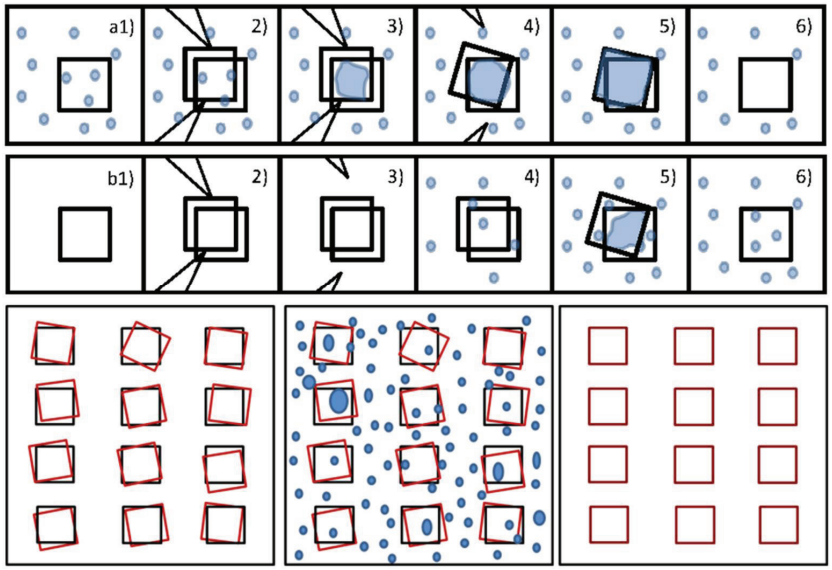

Fig.11 Water mist-first approach: (a1) water mist is delivered and water droplets fall onto the pattern and its surroundings. (a2) a micro handling tool carries a chip near the pattern. (a3) a meniscus is formed between the microchip when there is a contact between the chip and water droplet. (a4) - (a6) the chip is released and surface tension aligns the chip to the pattern according to the principle of minimum surface energy. Water mist-last approach: (b1) - (b2) A micro handling tool carries a chip near the pattern with a misplacement (bias). (b3) the chip is released. (b4) - (b6) water mist is delivered and water droplets fall onto both patterns and their surroundings, and the misplacement is corrected by surface tension driven self-alignment. (c) – (e) parallel water mist induced microassembly using water mist-last approach. Note: in the figure a tweezers type micro handling tool is used, which can be replace by any type of gripper or feeding mechanism.

One problem for the water mist-last approach is that reliable releasing cannot be guaranteed. The top chip may adhere to the micro handling tool and can easily tilt during releasing. This typical releasing problem in microassembly is possible to be solved using a vacuum micro gripper or other

parallel transferring methods, such as transfer printing [53], which can achieve a successful release with a reasonable accuracy.

Water mist induced hybrid microassembly technique has the benefits of the previously reported droplet assisted hybrid microassembly technique, while requiring less calibration and lower hardware requirements. It has potentially better scalability due to smaller droplet size. Furthermore, this technique can be an option for assembling micro components on patterned surfaces in parallel in the semiconductor industry, such as RFID tags assembly.

3.3 Hybrid microassembly with forced wetting

Hybrid microassembly requires well-designed pattern where the self-alignment process will occur. In the case of water as the self-alignment medium, the general rule is that the pattern should be hydrophilic and the substrate should be hydrophobic. It is challenging to use hydrophobic patterns for self-alignment because of its poor wettability with water. To tackle the problems of poor wetting with the hydrophobic pattern, two forced wetting methods have been developed. The two forced wetting methods are presented in **Fig.12** (a) and (b): (a) introduce an excessive amount of water, more than is needed for self-alignment and (b) force the water droplet to wet the hydrophobic patterns by pushing the chip against the pattern. The forced wetting in this thesis refers to the spreading of liquid on the pattern beyond what can be achieved by the wetting of the normal amount of water used in self-alignment.

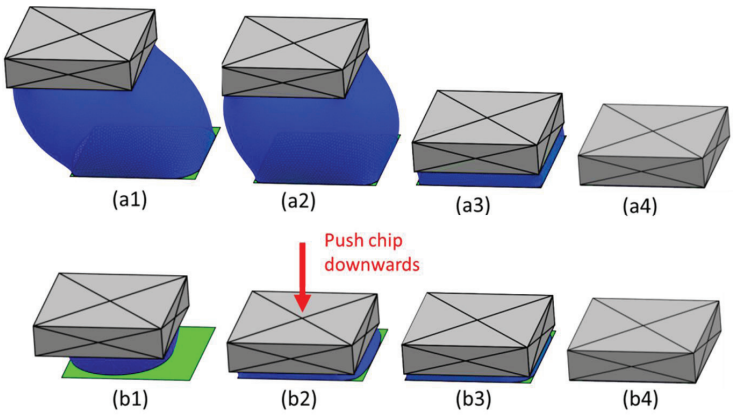

Fig.12 Numerical simulation of water droplet self-alignment of a microchip on a hydrophobic pattern with forced wetting, size of chip and hydrophobic pattern 200μm × 200μm, advancing contact angle and receding contact angle of water on pattern 118° and 69° respectively: (a1)-(a4) drop self-alignment with excessive amount of water (8 *nL*); (b1)-(b4) droplet self-alignment applying external pressure to force the water (0.9 *nL*) to wet the hydrophobic pattern, simulated using receding contact angle 69°.

As shown in **Fig.12** (a1)-(a4), the first forced wetting technique enables the water drop pinning at the edges of the patterns by dispensing excessive amount of water on the pattern. The second technique (**Fig.12** (b1)-(b4)) applies normal amount of water for self-alignment, but the water drop is forced to spread on the hydrophobic pattern by pushing the top chip against the pattern. Both forced wetting techniques lead to greater wetting area of the pattern and thus more successful self-alignment.

In the case of the first forced wetting technique, large amount of water (8 *nL*) is used (**Fig.12**). With excessive amount of water, the chip should align with the pattern due to the full wetting. The second forced wetting technique uses small amount of water (about 0.9 *nL*) and thus the surface of the pattern is only partly wetted (**Fig.12** (b1)). The gripper pushes the chip against the pattern and forces the water droplet to wet the pattern (**Fig.12** (b2)). Then the chip is released, and the surface tension drives the chip to align with the pattern (**Fig.12** (b3) and (b4)).

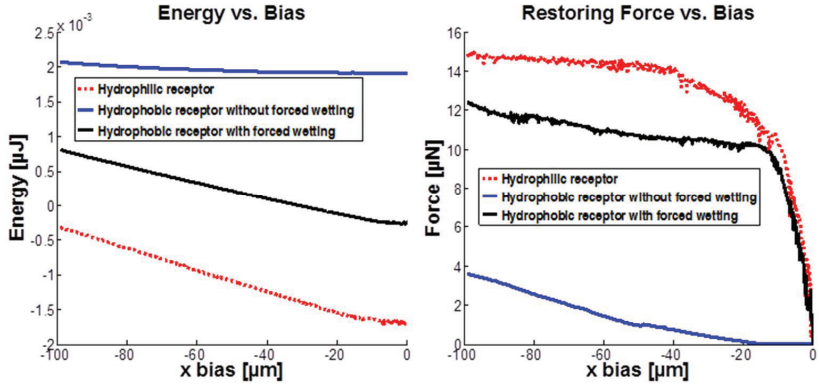

(a) (b)

Fig.13 (a) Energy and (b) restoring forces on hydrophilic receptor, hydrophobic receptor with forced wetting and hydrophobic pattern without forced wetting.

Fig.13 (a)-(b) compare the surface energy and restoring force of the self-alignment process with the same amount of water of 0.9 *nL* for three cases: 1) on a hydrophilic pattern (simulated using apparent contact angle of 30°); 2) on a hydrophobic pattern without forced wetting (simulated using advancing contact angle of 118°); 3) on a hydrophobic pattern with forced wetting (simulated using receding contact angle of 69°). **Fig.13** (a) shows that the receding contact angle of 69° leads to much larger value of restoring force compared with the much smaller forces created using advancing contact angle of 118°. In the case of pressing, much larger wetting reduces the effective contact angle to a value close to the receding contact angle after

the pressing was ended, and therefore the results of **Fig.13** (a)-(b) should also apply. The small amount of noises appeared in the restoring force curve (red curve) of **Fig.13** (b) are due to the numerical errors in simulation, which however does not affect the estimation of the level and trend of the force.

4. Patterns for Hybrid Microassembly

Droplet confinement on patterns is a key process in self-alignment and it can be achieved both on flat and protruded patterns. In case of a flat pattern, a droplet can be confined on the pattern based on large wetting contrast between the pattern and substrate. Self-alignment on protruded pattern uses geometrically solid edges as a boundary to prevent the liquid droplet spreading outside of the pattern. This section introduces the nano-structured and micro-patterned surface for droplet confinement in hybrid microassembly.

4.1 Oleophilic/ oleophobic nano-structured surface

4.1.1 Porous ormocer functionalized with fluorinated trichlorosilane

Droplet self-alignment with adhesives has the benefit of being able to make a permanent bonding. However, self-alignment using adhesive droplets in air is very challenging. The key of droplet self-alignment relies on the contact angle contrast, i.e., on the difference in contact angle, between the pattern and the substrate. Most adhesives are oil-like and they have low surface tension, which typically leads to a low contact angle on most surfaces. Consequently, for most adhesives, it is difficult to find a pattern and substrate that would lead to large enough contact angle contrast. Earlier work avoided the problem by using vertical solid edges to confine the droplet [27], which is not desirable in many applications. A new oleophilic/oleophobic nano-structured surface has been developed, where the oleophobic substrate is made of a topographical microstructure of porous ormocer functionalized with a fluorinated trichlorosilane and the oleophilic area consists of gold patterns. **Fig.14** shows a SEM image of the structure of the porous ormocer surface.

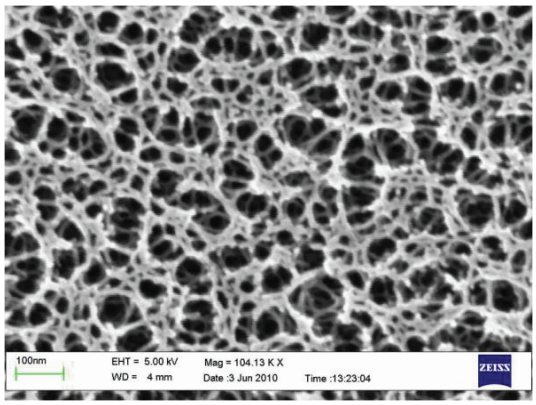

Fig.14 SEM image of the structure of the porous ormocer surface.

The fabricated oleophilic gold patterns are shown on the functionalized ormocer substrate in **Fig.15** (a). The wettability of the fabricated surface has been tested with both a normal cooking olive oil and a thermal adhesive (Delo 18507). The contact angle of the olive oil on the oleophobic part of the fabricated surface is measured as 133° as shown in **Fig.15** (b). Contact angles of the adhesive are measured as 53° on the oleophilic gold pattern of the surface as shown in **Fig.15** (c) and 119° on the oleophobic part of the fabricated surface as shown in **Fig.15** (d). This leads to a contact angle contrast of 66°.

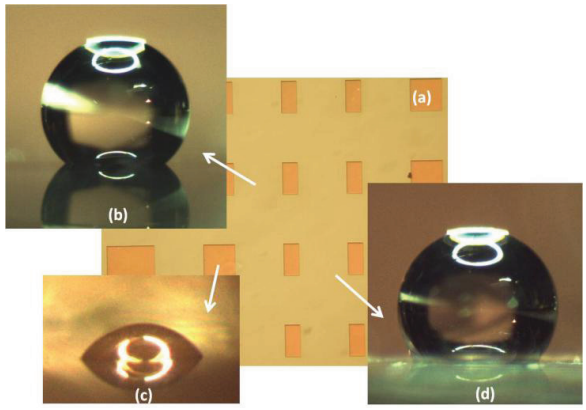

Fig.15 (a) Gold patterns of 50nm thickness on the ormocer substrate after functionalization with trichlorosilane; (b) Oil-drop-contact angle: 133° on oleophobic substrate; (c) Adhesive-drop-contact angle : 53° on oleophilic pattern; (d) Adhesive-drop-contact angle : 119° on oleophobic substrate.

4.1.2 Black silicon coated with fluoropolymer

To simplify the fabrication process of making oleophilic/oleophobic patterns, a simple and fast process has been developed. The process consists

of only one pass of photolithography, cryogenic deep reactive ion etching (RIE) and reactive ion etching steps to fabricate oleophilic/phobic patterns. **Fig.16** shows top and side view SEM images of the fabricated template with a fluoropolymer coating. In **Fig.16** (a), the patterns are seen as dark square patterns. The magnified view image is shown in **Fig.16** (b). The substrate surface consists of nano scale texture, which composes the surface roughness (see **Fig.16** (c)). **Fig.16** (d) shows that the pattern is protruded and has a well-defined boundary line with the substrate. The side view image of a fluoropolymer coated pattern (**Fig.16** (e) shows the geometry of the sharp solid edge and its height from the base of the needles (<4μm). The solid edge height is a combination of etched silicon, silicon dioxide thickness on the protruded pattern and fluoropolymer thickness.

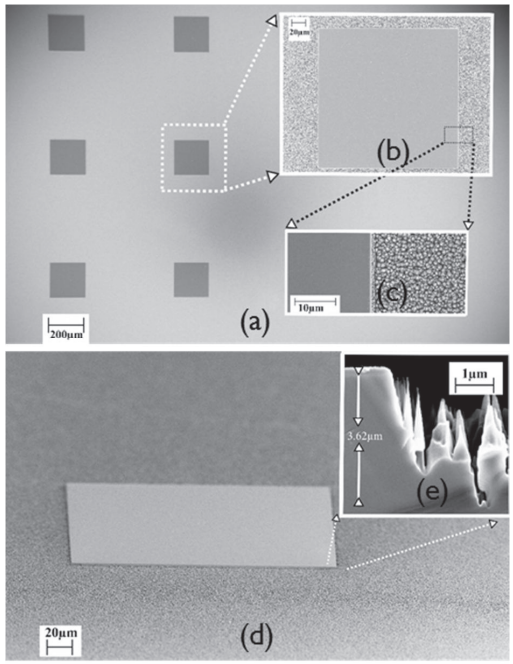

Fig.16 SEM images of a hybrid black silicon template: (a) Top view image showing patterns and black silicon substrate with a fluoropolymer coating; (b) Magnified view image of a pattern; (c) Top view image showing substrate surface with nano scale texture; (d) Side view image showing the height of the sharp solid edge and black silicon needles; (e) Magnified side view image showing the height of the solid edge.

Advancing contact angle measurements with water and adhesive are shown in **Fig.17**. The water contact angles were measured as 118° (**Fig.17** (a)) on the patterns and 179 ± 1° (**Fig.17** (c)) on the substrate, and adhesive contact angles were measured as 55° (**Fig.17** (b)) on the patterns and 110° (**Fig.17** (d)) on the substrate.

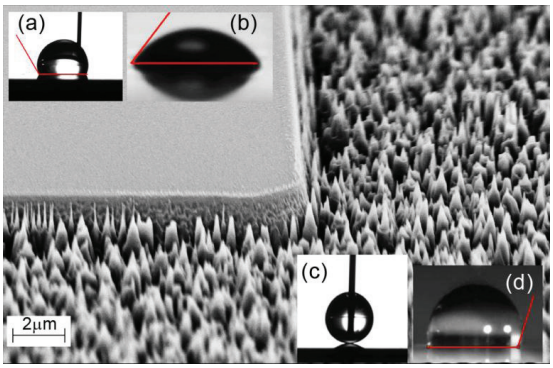

Fig.17 Advancing contact angle measurement of (a) Water droplet on a pattern: 118° (b) Adhesive droplet on a pattern: 55° (c) Water droplet on substrate: 179 ± 1° (d) Adhesive droplet on substrate: 110°.

High contact angle or low wettability of plane and homogenous patterns (**Fig.17** (a)) is attributed to the fluoropolymer coating. The low surface energy fluoropolymer coating changes the chemical composition of the surface, which makes it hard for the water droplet to spread on the surface and therefore the droplet exhibits a high contact angle. With adhesive, the patterns are more wettable (**Fig.17** (b)). Higher wettability with adhesive is due to the lower surface tension of adhesive (32.6 mN/m) compared to water (72 mN/m).

The reason for the superhydrophobicity of fluoropolymer coated black silicon substrate is that the substrate surface is non-homogenous and contains nano-scale black silicon needles. With the introduction of such roughness, the surface becomes inhomogeneous and the Young's equation [43] cannot be directly applied in this situation. In the case of inhomogeneous surface, two other models are normally used to explain the wetting behavior, i.e. Wenzel [44] or Cassie-Baxter [45]. On an intrinsically hydrophilic surface the introduction of roughness leads to increase in hydrophilicity, whereas, on hydrophobic surface the roughness increases hydrophobicity and the droplet usually assumes a Cassie-Baxter or composite state [45].

4.2 Hydrophilic/hydrophobic micro-patterned surface

4.2.1 Segmented patterns

In the RFID tag assembly or other low-pin count chip assembly, it is very common that there are several electrical contacts (bumps) on the chips as shown in **Fig.18**. Therefore, the pattern, or the pattern, is required to have a

segmented structure consisting of electrodes corresponding to electrical contacts on the chips.

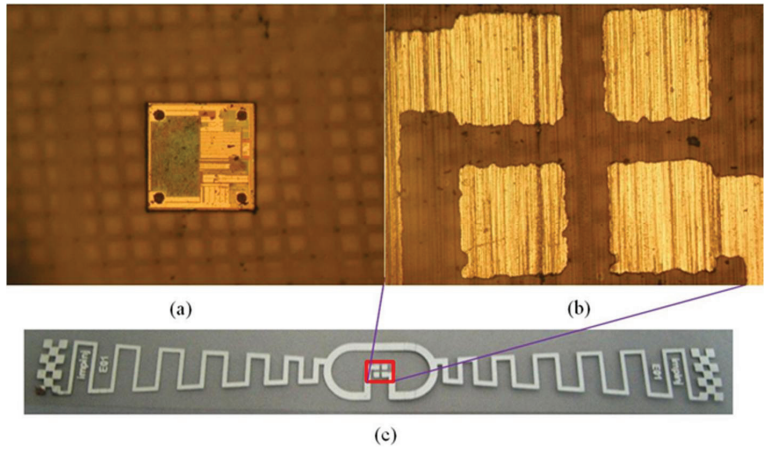

Fig.18 730μm × 730μm × 70μm RFID chips with four electrical contacts: (a) Top view of a RFID chip; (b) Zoomed image of four electrodes on a RFID antenna; (c) An RFID antenna.

To achieve self-alignment with water, the pattern should be hydrophilic and its substrate needs to be hydrophobic. In theory, the self-alignment process can easily reach energy minimum if the pattern has a non-segmented hydrophilic surface that matches the size of the RFID chips. However, such design would require an additional coating on top of the four pads, which brings complexity to the manufacturing process and an additional cost. Therefore, the patterns are designed in such a way that only the pads are hydrophilic while the gaps between the pads are of the same hydrophobic material as the substrate. For easy fabrication, the substrate is coated with Teflon and the pads are coated by SiO2. **Fig.19** shows the design and fabricated 730μm × 730μm pattern segmented into four pads with 100μm gap.

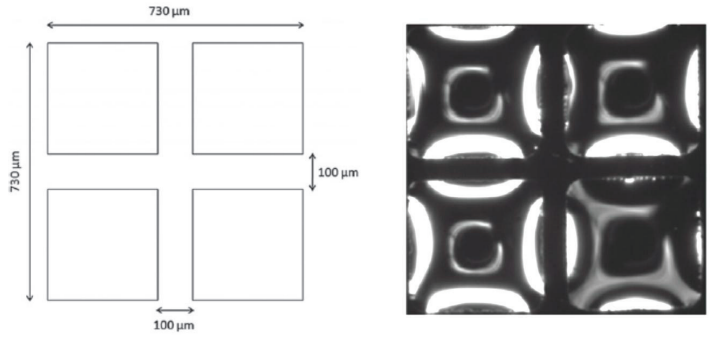

Fig.19 (a) Design of a segmented pattern with the gap size of 100μm and the pattern size of 730μm × 730μm. (b) The fabricated 4-pad segmented pattern with a water droplet confined on each pad.

The segmented pattern was tested with water. In the tests, the water is dispensed on each pad separately and the contact angle of the water is about 90◦ and 30◦ on the substrate and on the pads. Due to the surface energy difference between the hydrophilic pads and hydrophobic background, the water was kept well inside the pads and it didn't spread over the substrate.

4.2.2 Patterns with jagged edges

Many assembly processes, such as integration of RFID tags, are very cost sensitive. Therefore, low cost fabrication processes are often preferred, which result in patterns with features that are poorly defined. One of the phenomena is that the edges of the patterns have significant jaggedness as shown in **Fig.20**.

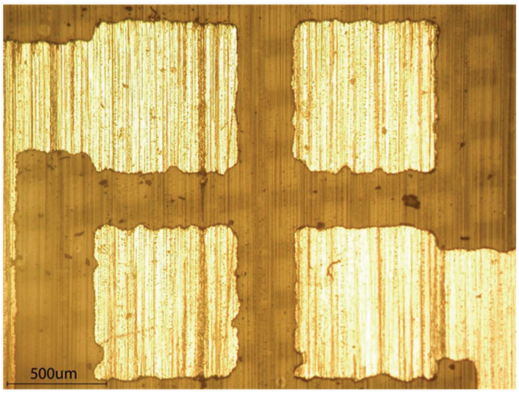

Fig.20 An example of real-world RFID antenna with significant edge jaggedness.

To design the low precision patterns for self-alignment tests with RFID microchips, we start with some real-world RFID antennas as shown in **Fig.20**, which contains four electrodes. It is obvious that each edge of the electrodes has significant jaggedness. Based on measurements, the maximum peak-to-peak value of the jaggedness is about 50μm, which is around 7% of the size of four electrodes (730 μm). However, the peaks are distributed sparsely and randomly on the edges. The peaks with large amplitudes, either outwards or inwards the patterns, are quite rare. In our design, we did not follow exactly the relative jaggedness of the real-world case for generality. The patterns are designed to have four segments, or pads, to mimic four electrodes. The dimensions of the whole pattern are 730 μm, similar to the size of RFID chip used in the test, which is 730 μm × 730 μm × 70 μm in average. The heights of the peaks of the jaggedness are presented using the values from normal distribution with standard deviations (std.) of

10μm and 5μm, resulting in maximum peak-to-peak value of 40 μm and 20 μm in 95% of the cases correspondingly.

To achieve self-alignment, the patterns are hydrophilic, and the background is hydrophobic. The fabrication process is the same as used for segmented patterns described in the last section. The substrate is coated with Teflon and the pads are coated by SiO2. **Fig.21** shows the design and fabricated patterns with jagged edges, where one can see that the jagged edges are similar to the real-world RFID antenna in **Fig.20**.

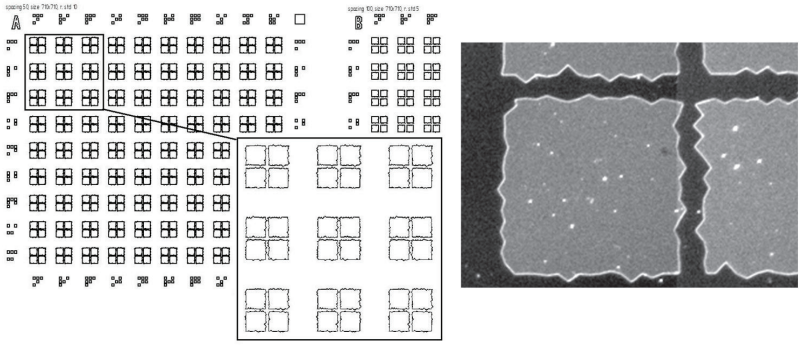

(a) (b)

Fig.21 (a) Design of the patterns with edge jaggedness of 10μm standard deviation and 40μm spacing; (b) 730μm x 730μm patterns with the jaggedness of 10μm standard deviation and 40μm spacing.

To further study the influence of the amplitude and pitch of the jagged edges on performance of self-alignment, two kinds of patterns with jagged edges have been designed as shown in **Fig.22**.

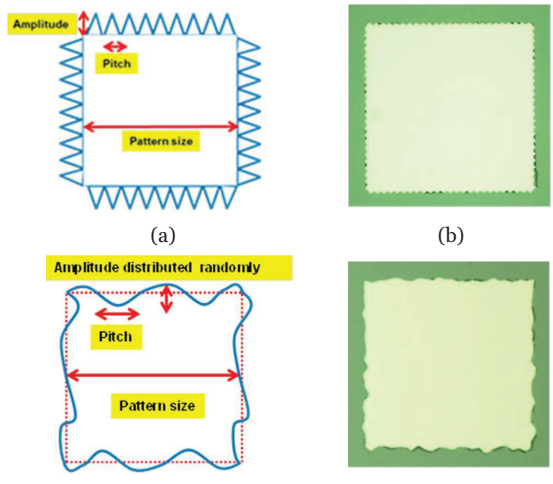

(a) (b)

(c) (d)

Fig.22 (a) Sketch of a pattern with regular jagged edges, (b) a fabricated 200μm x 200μm pattern with regular jagged edges of 4μm amplitude and 2μm pitch, (c) sketch of a pattern with random jagged edges, (d) a fabricated 200μm x 200μm pattern with random jagged edges of 2μm std of the amplitude and 8μm pitch.

One with regular edge jaggedness, which has spikes of the same size pointing outwards the pattern is shown in **Fig.22** (a) and **Fig.22** (b). The other with random edge jaggedness, which has spikes of random sizes following normal distribution with zero mean along the edges, is displaced in **Fig.22** (c) and **Fig.22** (d).

4.3 Patterns with geometric solid edges

When the pattern is hydrophilic, most of the liquids that can be considered for the self-alignment process will spread out of the pattern. Instead of making patterns hydrophilic and the substrate hydrophobic, another simple solution is to create a sharp edge around the pattern to trap the liquid inside the pattern. One of the simplest ways to create sharp edges is to fabricate protruded patterns. In the thesis, SU-8 was chosen because it is easy to fabricate relatively high aspect ratio patterns. The patterns are fabricated on a silicon substrate. Standard SU-8 lithography (spin coating, baking, exposure, development, and hard-baking) is used to make the patterns. **Fig.23** shows a SEM image of a square-shaped SU-8 pattern with the dimension 200 × 200 × 30μm.

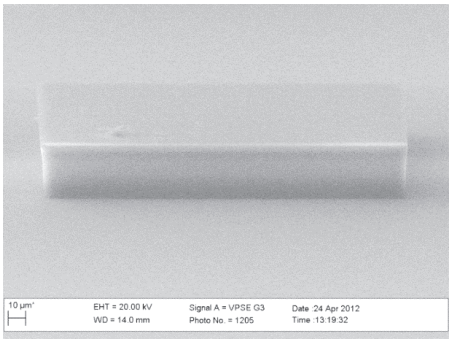

Fig.23 SEM image of a fabricated SU-8 pattern with size of 200μm×200μm×30μm.

5. Results and Discussions

This section summarizes the main results of the publications. The section consists of 7 sub-sections, and the first sub-section introduces the system set-up for all the experiments, and the rest of the section is divided into 6 sub-sections.

5.1 Experimental set-up

The hybrid microassembly experiments were carried out using a microassembly setup consisting of an assembly system (pick-and-place), a dispensing system and an imaging system as shown in **Fig.24**. The assembly system contains a custom-built microgripper mounted on a motorized linear stage (Physik Instrumente M111.1DG) for vertical movement; a sample carrier mounted on a short range motorized linear stage (Physik Instrumente M-122.2.1DD) for motion in x-axis and a long range motorized linear stage (Physik Instrumente M-404.8PD) for motion in y-axis between assembly site and dispensing site. The dispensing system consists of a water droplet dispenser and an adhesive droplet dispenser, where water dispenser is mounted in about 45° angle at the assembly site and the adhesive dispenser is mounted vertically at the dispensing site. The water droplet dispenser is a noncontact dispenser (Gesim/PicPIP), actuated by a piezoelectric diaphragm and can dispense droplets at a distance of a few millimeters. The amount of the liquid can be adjusted in the range of 100–400 picolitres. The adhesive droplet dispenser is an air-powered contact dispenser (EFD Mikros pen system), which can deposit droplets as small as 50 μm in diameter. The imaging system consists of a top-view microscope (Edmund/VZM1000i) and a side-view microscope (Edmund/VZM1000i) mounted at the assembly site, a top-view microscope (Edmund/VZM300i) and a side-view microscope (Edmund/VZM300i) mounted at the dispensing site.

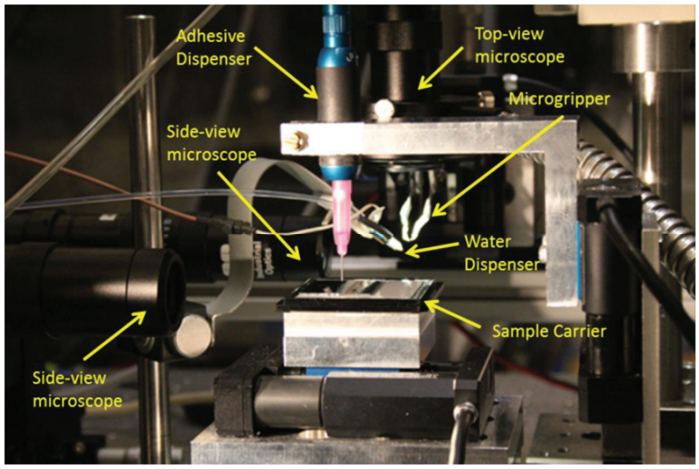

Fig.24 Hybrid microassembly system, which consists of a sample carrier, a microgripper, a water dispenser, an adhesive dispenser, two side-view microscopes and one top-view microscope.

5.2 Self-alignment on hydrophobic patterns (PUB1)

One key aspect of the hybrid microassembly is a well-designed pattern where the self-alignment process will take place. For example, if water is used for self-alignment, it is preferable that the pattern is hydrophilic against the hydrophobic substrate. However, in many applications, the patterns are made of hydrophobic materials, and it is an open question if the hydrophobic patterns can be used for self-alignment. **PUB1** investigates the self-alignment on a hydrophobic pattern and water using two forced wetting techniques. A nano-structured black silicon surface functionalized with fluoropolymer was used as a super-hydrophobic substrate, while the silicon dioxide pattern covered with fluoropolymer was served as the hydrophobic pattern. Contact angle of the water is 118° and 180° on the pattern and on the substrate respectively.

PUB1 reports droplet self-alignment on hydrophobic patterns using two forced wetting techniques: (a) introducing an excessive amount of water and (b) applying external pressure, which are shown in **Fig.25** and **Fig.26**. **Fig.25** (a-d) shows the frames of the self-alignment processes for an assembly case of a 200 μm × 200 μm × 50 μm chip on a 200μm × 200μm pattern using excessive amount of water (8 *nL*). Such large amount of water is sufficient to fully wet the surface of the pattern, and moreover the water is still well confined inside the pattern due to super-hydrophobicity of the substrate. The amount of water increases significantly when compared to the amount (0.4nL – 1.5nL) used to fully wet the same sized hydrophilic pattern. Self-alignment has been observed using this technique. **Fig.26** shows the

frames of the self-alignment processes for an assembly case of a 200 μm × 200 μm × 50 μm chip on a 200 μm × 200 μm pattern using external pressure. Small amount of water (0.9 *nL*) is dispensed on the pattern, and the surface of the pattern is partly wetted (**Fig.26** (a)). The microgripper moves the chip towards the pattern and forces the water droplet to wet the pattern (**Fig.26** (b)). Then the chip is released (**Fig.26** (c)), and the surface tension drives the chip to align with the pattern (**Fig.26** (d)). The external pressure can be easily controlled by adjusting the releasing position of the chip, and thus there is little additional requirement on the robot handling process.

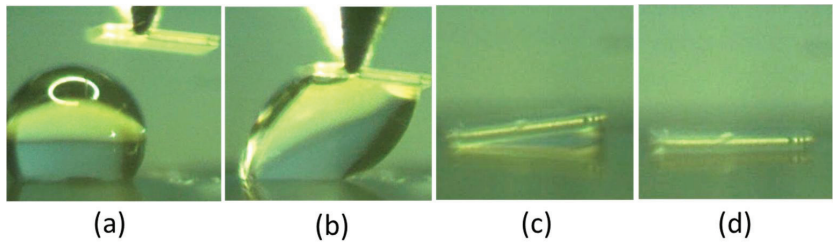

Fig.25 Self-alignment of a 200 μm × 200 μm × 50 μm SU-8 chip on the corresponding pattern using excessive amount of water.

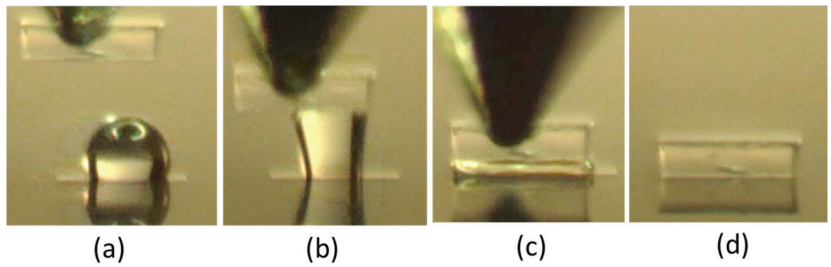

Fig.26 Self-alignment of a 200 μm × 200 μm × 50 μm SU-8 chip on the corresponding pattern using external pressure.

Both forced wetting techniques have been demonstrated for self-alignment using hydrophobic patterns, however they do require the super hydrophobic substrate to ensure the water confinement inside the pattern. To relax the requirement of super hydrophobicity of the substrate, hydrophobic patterns with sharp edges can also be used, which can also stop the liquid from spreading outside the pattern.

5.3 Self-alignment using adhesive in air (PUB2, 5)

Adhesives are commonly used for permanent bonding in microassembly. However most of the adhesives have low surface tension, and thus it is difficult to find a pattern and substrate that would lead to large enough contact angle contrast. **PUB2** reports a topographical microstructure of porous ormocer functionalized with a fluorinated trichlorosilane for the oleophobic area and gold patterns for the oleophilic area. The

oleophilic/oleophobic patterns show significant wettability contrast for adhesive (Delo 18507), with a contact angle of 119° on oleophobic part and 53° on the oleophilic part. Self-alignment of SU-8 microchips on the oleophilic/oleophobic patterns has been demonstrated in **Fig.27**. The final alignment accuracy is inspected using optical microscope by measuring the difference between the geometrical centers of the chip and the pattern. The accuracy is estimated to be less than 1 μm in x axis and 3.5 μm in y axis, where the measurement of this accuracy is limited by the accuracy of the microscopes. The self-alignment process takes about 500ms, which is about ten times longer than the self-alignment with same amount of the water. This is partly caused by the high viscosity (400mPa•s) of the adhesive, which increases both the time for wetting a pattern and reduces the restoring force in self-alignment [54]."

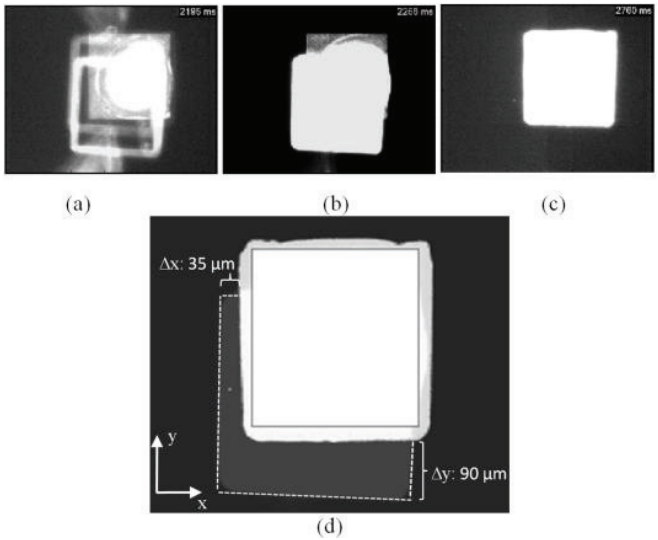

Fig.27 Self-alignment frames of a 200μm × 200μm × 50μm SU-8 chip on the corresponding gold patterns. (a) The chip is moving towards the pattern. (b) Release the SU-8 chip with a releasing bias of 90 μm and 35 μm in x and y axis individually. (c) Self-alignment is realized. (d) The super imposed image of (b) and (c), where the contour of the chip at the releasing position is highlighted with white dashed lines and the contour of the pattern is highlighted with dark line.

PUB5 reports the self-alignment of microchips on a simple-to-fabricate hybrid template with both water and UV-curing adhesive (EPO-TEK® UVO-114). The hybrid template consists of a nanostructured black silicon surface functionalized with fluoropolymer as a substrate and silicon dioxide covered with fluoropolymer as pattern. **Fig.28** shows optical microscope images of adhesive self-alignment of a SU-8 microchip on a pattern. The process was recorded from both top (**Fig.28** (a, b, c)) and side (**Fig.28** (d, e, f)). The amount of the adhesive droplet was carefully controlled with the adhesive

dispenser and 0.4 *nL* adhesive has been used in the tests. The accuracy of the self-alignment is seen in **Fig.29** (a, b). The microchip is released with a large initial bias as shown in **Fig.29** (a) (50 μm in x-axis, 40 μm in y-axis, 50 μm in z-axis, 60% overlapping area). The measured alignment accuracy is 1.2 μm in x-axis, 2.3 μm in y-axis. The self-alignment process was completed in less than 110 milliseconds.

The reported oleophilic/oleophobic patterned surface and hybrid template provide promising solutions for droplet self-alignment of micro parts using commercial adhesives in ambient air environment. This may lead to potential applications in packaging of semiconductor devices and 3D integration of the micro devices, where adhesives are extensively used.

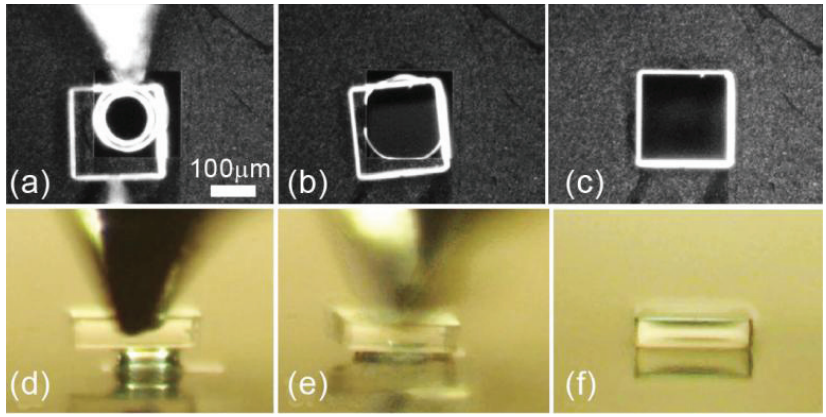

Fig.28 Self-alignment sequences with adhesive. (a, d) The SU-8 microchip is ready to be released with the predefined initial bias, (b, e) the microchip is released (c, f) the microchip is aligned with the pattern.

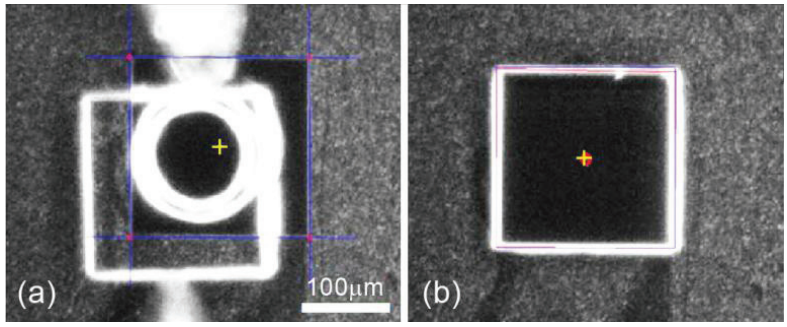

Fig.29 Measurement of the self-alignment accuracy with adhesive. (a) A SU-8 microchip is released to the same sized pattern, with a large initial bias (50 μm in x-axis, 40 μm in y-axis, 50 μm in z-axis, 60% overlap). (b) The self-aligned microchip with accuracy of 1.2 μm in x-axis, 2.3 μm in y-axis.

5.4 Self-alignment on segmented patterns (PUB3, 9)

It is common in many applications that the pattern consists of segmented structures corresponding to the electrical contacts on the chips. **PUB3** and **PUB9** report an in-depth study of water droplet self-alignment technique that self-aligns radio frequency identification (RFID) chips on four-pad segmented patterns. For an easy fabrication, the substrate is coated with Teflon and the pads are coated by SiO2. As a result, patterns consists of four hydrophilic pads on a hydrophobic background are obtained. The influences of the key parameters, such as bias and gaps have been investigated in theory and experimentally. The gap is the spacing between two pads. The size of the pattern is 730×730μm, which is the same as the size of the RFID chip.

The self-alignment process of a RFID chip on a segmented pattern with four pads is simulated using *Surface Evolver*. **Fig.30** displaces the surface energy of water meniscus on the segmented pattern with gap size of 50μm and 100μm, with respect to the bias in x direction. The simulation indicates the largest allowable bias with 50μm and 100μm gaps are 380μm and 350μm, which is about 52% and 48% of the size of the pattern correspondingly.

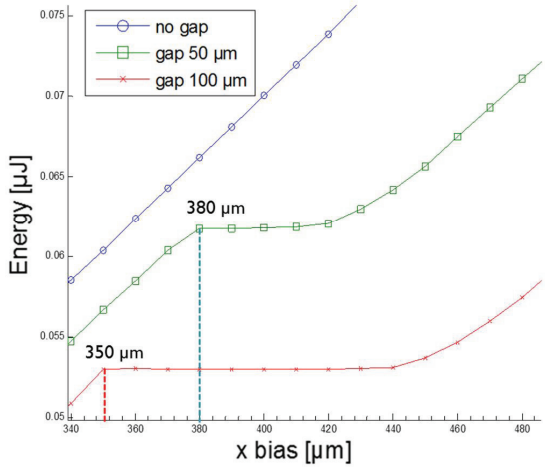

Fig.30 Surface energy of water meniscus with respect to the x bias using 730μm × 730μm segmented patterns with two different gap sizes: 50μm and 100μm.

A series of experiments have been carried out to check the yield of the self-alignment of different biases and gaps, including 50μm and 100μm and larger gaps up to around 400μm. The yield is the proportion of a successful alignment out of all tests of a particular initial bias and gap. A successful alignment is defined as an alignment where the error is indistinguishable under the optical microscope used in the tests. The x bias and y bias are varied in the range of 0μm to 400μm. The yield as a function of the parameters is shown in Table 1. For each setting, the test is repeated for 5

times. The results show that 100% yield can be achieved with bias less than 400μm in one axis and no obvious difference with 100μm gap and with 50μm gap regarding the yield of the self-alignment.

Table 1 Yield vs. Gaps

	50μm gap	100μm gap
x-bias, y-bias	yield	yield
50μm,0 μm	100%	100%
100μm,0 μm	100%	100%
300μm,0 μm	100%	100%
400μm,0 μm	100%	100%
500μm,0 μm	80%	60%
600μm,0 μm	0%	0%
50μm,50 μm	100%	100%
100μm,100 μm	100%	100%
200μm,-200 μm	80%	100%
300μm,-300 μm	20%	20%

Fig.31 shows one example of a successful alignment using 730μm × 730μm patterns with 100μm gap.

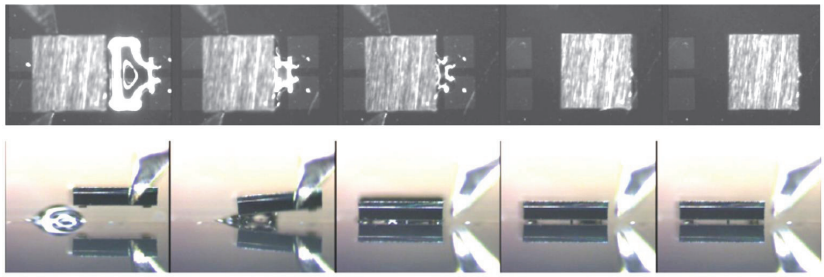

Fig.31 Top view and side view of water droplet self-alignment of a 730μm × 730μm RFID chip on a segmented pattern with 100μm gap. The initial bias is 300μm in the x-axis.

Patterns with larger gap 205 μm and 405 μm were also tested with small bias in both x and y-axis. Each test has been repeated 15 times. With 205 μm, although the bias is rather small compare to the size of the pattern (about 10 % of the size of the pattern) in both x and y axis, possibility of error seems to increase due to the large gap. However the successful alignment was still possible with a yield of 73 %. **Fig.32** shows that a successful alignment is still possible when the gap increases to 405μm, although the gap is so large that the droplet is not able to even touch the pads before the RFID chip on the top makes the water spread. **PUB3** reported large variations (20ms – 250ms) in the self-alignment speed, this may be caused by the difference in releasing, or the volume and the position of the dispensed liquid. Those factors can lead to a very different wetting process and consequently the dynamics of the self-alignment process can be very different from test to test.

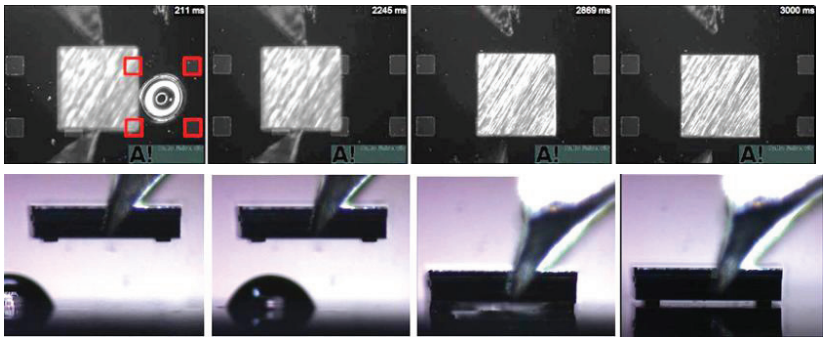

Fig.32 Top view and side view of water droplet self-alignment of a 730 × 730μm RFID chip on an segmented pattern with 405μm gap, the initial bias is 40μm in both x and y axis. The outline of the segmented pattern is highlighted with red lines.

In summary, both theory and experiments indicate that the self-alignment between the 730μm × 730μm RFID chips and the segmented pattern can be achieved when the initial bias is as large as 50% of the size of the chip. Although the thesis only investigates the four-pad segmented pattern, self-alignment on the patterns with more pads should be possible using water or another liquid, if the size of the whole pattern is same as the chip and the liquid is able to confine inside the pattern. The result provides a solid basis for the design of future self-assembly or droplet self-alignment process for RFID or other chips with multiple electrical contacts.

5.5 Self-alignment with water mist (PUB4, 6, 10)

Water mist used as the liquid for self-alignment brings many benefits, such as lower hardware requirements, better scalability due to the smaller droplet sizes and potential parallel assembly. The experimental tests were performed using the hybrid microassembly system discussed in 5.1.

To deliver the water mist to the test samples, two silicone tubes with inner diameter 6 mm and outer diameter 9 mm are connected to the exit of a humidifier. The ends of the tubes are placed near the sample carrier from two opposite directions to spread the water mist evenly on the samples as shown in **Fig.33**.

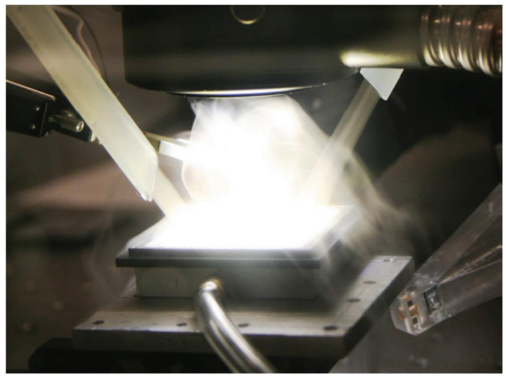

Fig.33 Hybrid microassembly system with water mist.

PUB4 investigates the droplet forming process using machine vision, where each individual droplet on the microchip surface can be identified and the volume per surface area can be calibrated at a specific time. The result reveals that the volume of water droplets on the alignment surface grows linearly as a function of time as shown in **Fig.34**. The volume of the droplets in **Fig.34** starts to grow after 1.87 s because of the delay in the silicon tubes.

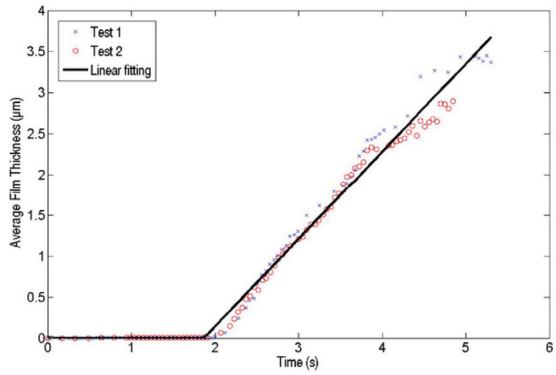

Fig.34 Linear water droplets accumulation process.

PUB4 investigates the maximum tolerance of the initial placement error in alignment of SU-8 chips 200μm × 200μm × 70μm in size (see **Fig.35**).

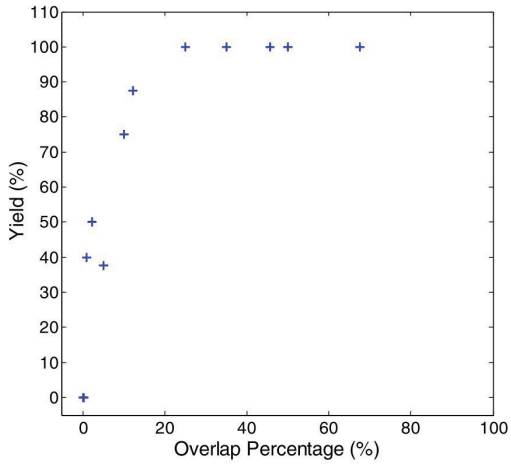

Fig.35 Alignment yields versus overlap percentage between the bottom chip and the top chip with the same dimension.

The overlapping area between the lower chip and the top chip can be calculated based on the x-bias and the y-bias. **Fig.35** shows that the overlapping area between the lower chip and the top chip correlates with the alignment yield. 100% yield can be achieved when the overlapping area is greater than 25% of the size of the chip. Even when the overlapping area is only 5%, 40% yield can still be reached. One demonstration of successful self-alignment with rather large bias is shown in **Fig.36**.

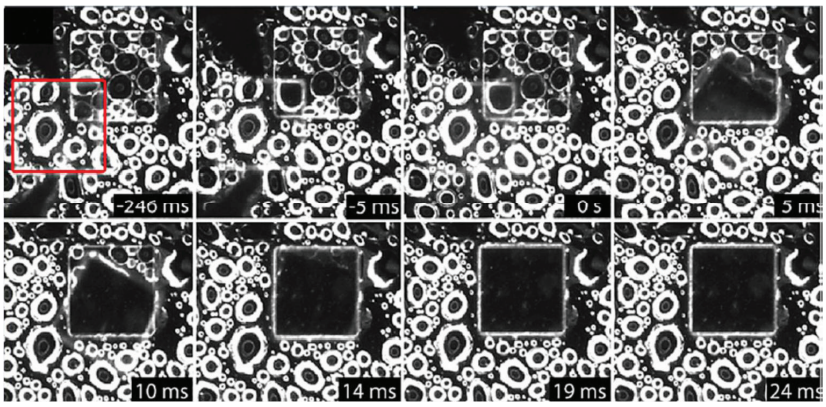

Fig.36 Self-alignment of SU-8 chips of the same size. The x-axis bias is −130 μm and y-axis bias is −130μm. Moreover, time tags of each image frame are shown. The time 0 is when the microgripper releases the chip.

PUB4 also reports the possibility of stacking two SU-8 chips of different dimensions as shown in **Fig.37**.using the proposed self-alignment technique

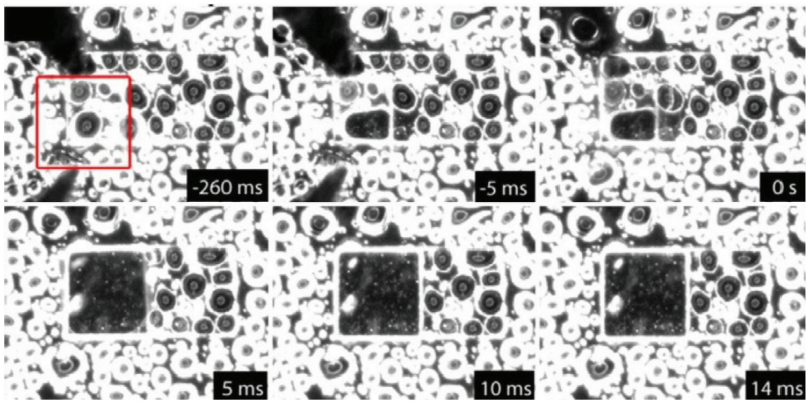

Fig.37 Self-alignment of SU-8 chips of different sizes, top chip: 200 × 200 × 70μm, bottom chip: 200 × 400 × 70μm, biases in x-, y- and z-axes: −65, −65 and 20μm, correspondingly.

PUB6 reports the first demonstration of the self-alignment with water mist for parallel assembly. **Fig.38** (a-c) presents parallel alignment of 20 and 30 pairs of misaligned microchips using droplet self-alignment with water mist. The deposition of water mist plays important role in the self-alignment, and the uneven distribution will cause a time delay between the self-alignment of different chips. It may end up with some of the chips aligning and some of the chips failing to align. Therefore, the water mist deposition process needs to be calibrated to achieve relatively uniform deposition, so that all the chips can align simultaneously.

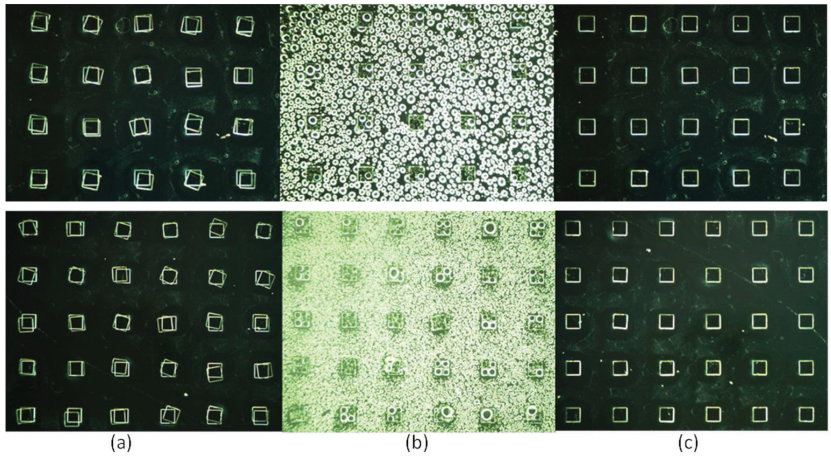

Fig.38 Parallel alignment of 20 pair of microchips using droplet self-alignment with water mist: (a) 200μm x 200μm x 30μm chips are placed on the top of a matrix of 20 patterns of the same size with random placement error; (b) water droplets are delivered in the form of the water mist; (c) the placement errors are corrected and all the chips are aligned with the patterns.

In summary, the results show that the proposed technique is a promising solution for assembly of microchips. This technique can be applied to both parallel self-assembly and robotics-based hybrid assembly. This technique can be an option for assembling micro components on patterned surfaces in

the semiconductor industry, such as RFID tag assembly. To utilize this technique for RFID assembly, the patterns should be carefully designed due to the fact that the water-mist-induced droplets do not only land on the patterns but also on the substrate. The height difference between the patterns and substrate should be taken into account when designing the process.

5.6 Self-alignment on patterns with jagged edges (PUB7, 8)

Low cost fabrication processes result in micro components with features that are poorly defined and with defects. **PUB7** reports the influence of the dimension and the edge jaggedness on the yield and accuracy of the droplet self-alignment with water, using 730 × 730 × 70μm RFID chips as the test samples. Hydrophilic/phobic patterns with SiO_2 served as the pattern and Teflon as the substrate were fabricated to create wetting contrast for water.

The self-alignment occurs with proper releasing bias, despite the variation in size of the pattern and edge jaggedness. However variation in size could affect the alignment accuracy. The better the size of the pattern matches the chip, the higher the alignment accuracy can be received. For example, the self-alignment accuracy with a 730μm × 730μm chip was clearly better for 710 μm × 710 μm patterns with edge jaggedness of standard deviation 10 μm than 710 μm × 710 μm patterns without edge jaggedness. **PUB8** reports the exact relationship between various parameters of jagged edges and the alignment accuracy of 200μm × 2000μm microchips on patterns with jagged edges.

The alignment accuracy is calculated by measuring the difference between the geometry centers of the chip and the pattern after the self-alignment is finished as shown in **Fig.39**.

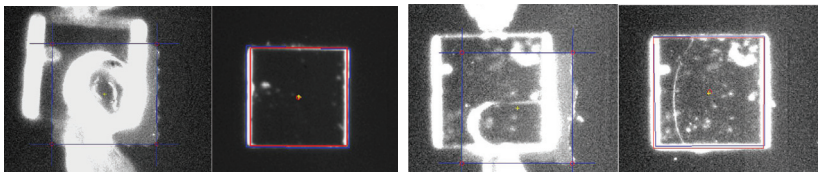

Fig.39 Droplet self-alignment on patterns with regular jagged edges and with random jagged edges: Four edges of a pattern are highlighted with blue lines and center of the pattern marked with a yellow cross. Four edges of a chip are highlighted with red lines and center of the chip marked with a red circle.

An image analysis based method is implemented using Matlab for detection of the geometry centers. The results show that self-alignment can be achieved on the patterns with regular edge jaggedness as well as with random edge jaggedness. The alignment accuracy decreases as the amplitude of the edge

jaggedness increases. However, high alignment accuracy of 2μm can still be achieved even with the edge jaggedness as large as 8μm. Large standard deviation (STD) in the measurement has been observed, which is due to the limited resolution of the optical microscope.

The results indicate that self-alignment occurs repeatedly with proper releasing bias, despite the variation in size of the pattern and edge jaggedness. Variation in size could affect the alignment accuracy. The better the size of the pattern matches the chip, the higher the alignment accuracy can be obtained. Self-alignment can be achieved on the patterns with regular edge jaggedness as well as with random edge jaggedness alignment. Accuracy decreases as the amplitude of the edge jaggedness increases. Alignment accuracy of 2μm can still be achieved with the edge jaggedness as large as 8μm.

6. Conclusions

Hybrid microassembly technique utilizes the fast-speed robotic handling tool for the coarse positioning and applies droplet self-alignment technique to achieve high-accuracy alignment. By combing both the robotic pick-and-place technique and droplet self-alignment technique, hybrid microassembly technique can achieve high speed and high precision simultaneously. As reported in the related publication of this thesis work [42], throughput over 40,000 unit per hour has been demonstrated with micron accuracy.

This thesis assesses the adaptability of hybrid microassembly by investigating three different hybrid microassembly handling strategies: 1) droplet assisted hybrid microassembly, 2) water mist induced hybrid microassembly and 3) hybrid microassembly with forced wetting. The results indicate:

- Droplet assisted hybrid microassembly is promising for stacking of microchips and self-alignment of microchips on patterns with water or adhesive.
- Water mist induced hybrid microassembly can be used for parallel self-alignment in the air. Alignment occurs if volume of the water mist is controlled with a uniform deposition. Alignment accuracy can reach sub-micrometer range.
- Hybrid microassembly with forced wetting can achieve self-alignment on hydrophobic pattern with super-hydrophobic substrate using two forced wetting techniques: introducing excessive amount of water or applying external pressure to force the water to wet the hydrophobic patterns.

The thesis investigates what kind of micro parts and patterns are suitable for hybrid microassembly. Five different types of patterns have been investigated for hybrid microassembly technique: (1) oleophilic/phobic patterns, (2) hydrophobic/super-hydrophobic patterns, (3) segmented patterns and (4) patterns with jagged edges, (5) patterns with sharp solid edges. The key results are summarized as follows:

- Oleophilic/phobic patterns are suitable for droplet self-alignment using adhesives in ambient air environment.

- It is possible to achieve self-alignment with both water and adhesive droplet using hydrophobic/super-hydrophobic patterns.
- Self-alignment occurs between microchips and segmented patterns with suitable initial bias as large as 50% and gap less than 10% of the size of the pattern.
- Self-alignment can be achieved on patterns with regular edge jaggedness as well as with random edge jaggedness. The alignment accuracy decreases as the amplitude of the edge jaggedness increases.
- The solid sharp edges around the pattern are easy to fabricate and an effective solution to confine the liquid inside the pattern and achieve self-alignment.

The above discussed handling strategies and patterns provide a good set of candidates for different potential applications. In some applications, such as integration of VCSELs (vertical-cavity surface-emitting laser) and RFID tag assembly, segmented planar patterns may be more suitable with the component design where each pin corresponds to an individual segment of the pattern. In some other applications, e.g. die-to-substrate assembly, patterns with solid sharp edges may be more suitable in confining the bonding adhesive. Therefore, this thesis explores different possibilities for potential applications, instead of seeking an optimal design for practical industry relevant applications, which can be topics of further research.

In the same spirit, robotic sequential feeding is the main methodology used in the thesis. Serial feeding allows quantitative study of the influence of the process parameters of e.g. pattern design, liquid medium, and initial releasing conditions on the results of hybrid microassembly. With the knowledge of the process parameters obtained, the process can be easily extended by replacing robotic serial feeding with more high-throughput feeding techniques, e.g. transfer printing or other parallel pick-and-place techniques. Already in the thesis, parallel mist self-alignment has been demonstrated in Section 5.5, which shows the extensibility of the research. Parallel microassembly with water mist is really promising for assembling micro components on patterned surfaces in parallel in the semiconductor industry. It can reach high precision microassembly at high yield, which is not achievable with the robotic microassembly technique.

There are two major failure modes observed in the hybrid microassembly process: 1) failed liquid confinement and 2) insufficient wetting. To avoid the failure, the amount of the liquid should be controlled in a reasonable range, and it should be sufficient to wet the pattern but still be able to confine inside the pattern. However, this range is not very sensitive, for example, in water droplet assisted hybrid microassembly of 300μm × 300μm SU-8 chips on

same sized SU-8 chips, over 98% yield is achieved when the droplet volume is between 0.9 - 3.1nL [39].

In conclusion, hybrid microassembly is a promising technology to improve the performance of current robotic systems. This thesis shows that hybrid microassembly is adaptable to large varieties of patterns. Several new hybrid microassembly handling strategies are developed and demonstrated. Such a wide adaptability and a variety of the processes indicate that hybrid microassembly can be a very promising approach for many potential applications, such as integration of surface emitting lasers, integration of small dies and 3D integration of chips with high density pin counts.

References

[1] K. Bohringer, K. Fearing, and K. Goldberg, “Microassembly,” in *Handbook of Industrial Robotics, Second Edition*, John Wiley & Sons, Inc., Hoboken, NJ, USA, 2007.

[2] M. Wautelet, “Scaling laws in the macro-, micro- and nanoworlds,” *European Journal of Physics*, vol. 22, no. 6, pp. 601–611, Nov. 2001.

[3] R. Fearing, “Survey of sticking effects for micro parts handling,” in *Proc. IEEE/RSJ Int. Conf. Intelligent Robots & Systems*, 1995, vol. 2, pp. 212–217.

[4] N. Dechev, W. Cleghorn, and J. Mills, “Microassembly of 3-D microstructures using a compliant, passive microgripper,” *Journal of Microelectromechanical Systems*, vol. 13, no. 2, pp. 176–189, 2004.

[5] Q. Zhou and P. Korhonen, “6 DOF dexterous microgripper for inspection of microparts,” in *Proc. IEEE/ASME International Conference on Advanced Intelligent Mechatronics*, 2005, pp. 534– 539.

[6] C. Clévy and N. Chaillet, “Micromanipulation and micro-assembly systems,” in *Proc. IEEE/RAS International Advanced Robotics Programm*, 2006.

[7] G. Yang, J. Gaines, and B. Nelson, “A supervisory wafer-level 3D microassembly system for hybrid MEMS fabrication,” *Journal of Intelligent & Robotic Systems*, pp. 43–68, 2003.

[8] J. Cecil, D. Powell, and D. Vasquez, “Assembly and manipulation of micro devices—A state of the art survey,” *Robotics and Computer-Integrated Manufacturing*, vol. 23, no. 5, pp. 580–588, Oct. 2007.

[9] “Datacon 8800 FC Quantum,” 2013. [Online]. Available: http://www.besi.com/files/Datacon 8800 FC Quantum.pdf4d5d0c9119407/Datacon 8800 FC Quantum.pdf.

[10] “SET-SAS FC 300R,” 2013. [Online]. Available: http://www.set-sas.fr/file/set-fc300r-a4-bd.pdf.

[11] F. Arai, D. Andou, Y. Nonoda, T. Fukuda, H. Iwata, and K. Itoigawa, “Integrated microendeffector for micromanipulation,” *IEEE/ASME Transactions on Mechatronics*, vol. 3, no. 1, pp. 17–23, Mar. 1998.

[12] E. Shimada and J. Thompson, “Prototyping millirobots using dextrous microassembly and folding,” in *Proc. ASME Symposium on Microrobotics ASME Intl Mech Eng Cong and Expo*, 2000, pp. 1–8.

[13] Q. Zhou, A. Aurelian, B. Chang, C. del Corral, and H. N. Koivo, “Micro assembly station with controlled environment,” *Journal of Micromechatronics*, vol. 2, no. 3–4, pp. 227–248, 2004.

[14] J. Feddema, P. Xavier, and R. Brown, “Micro-assembly planning with van der Waals force,” in *Proc. IEEE International Symposium on Assembly and Task Planning*, 1999, pp. 32–38.

[15] D. Haliyo, Y. Rollot, and S. Régnier, “Dynamical strategies for micromanipulation by adhesion,” in *Proc. SPIE, Microrobotics and Microassembly III*, 2001, vol. 261.

[16] H.-J. J. Yeh and J. S. Smith, “Fluidic self-assembly for the integration of GaAs light-emitting diodes on Si substrates,” *IEEE Photonics Technology Letters*, vol. 6, no. 6, pp. 706–708, Jun. 1994.

[17] U. Srinivasan, D. Liepmann, and R. T. Howe, “Microstructure to substrate self-assembly using capillary forces,” *Journal of Microelectromechanical Systems*, vol. 10, no. 1, pp. 17–24, Mar. 2001.

[18] J. Fang and K. F. Böhringer, “Parallel micro component-to-substrate assembly with controlled poses and high surface coverage,” *Journal of Micromechanics and Microengineering*, vol. 16, no. 4, pp. 721–730, Apr. 2006.

[19] C. J. Morris, S. Member, S. A. Stauth, and B. A. Parviz, “Self-assembly for microscale and nanoscale packaging: steps toward self-packaging,” *IEEE Transactions on Advanced Packaging*, vol. 28, no. 4, pp. 600–611, 2005.

[20] X. Xiong and Y. Hanein, “Multi-batch micro-self-assembly via controlled capillary forces,” in *Proc. IEEE/RSJ Int. Conf. Intelligent Robots & Systems*, 2001, vol. 3, pp. 1335–1342.

[21] U. Srinivasan and M. Helmbrecht, “Fluidic self-assembly of micromirrors onto microactuators using capillary forces,” *IEEE Journal of Selected Topics in Quantum Electronics*, vol. 8, no. 1, pp. 4–11, 2002.

[22] E. Saeedi, S. Kim, and B. a Parviz, “Self-assembled crystalline semiconductor optoelectronics on glass and plastic,” *Journal of Micromechanics and Microengineering*, vol. 18, no. 7, p. 075019, Jul. 2008.

[23] C. Lin, F.-G. Tseng, and C.-C. Chieng, “Orientation-specific fluidic self-assembly process based on a capillary effect,” *Journal of Micromechanics and Microengineering*, vol. 19, no. 11, p. 115020, Nov. 2009.

[24] R. J. Knuesel and H. O. Jacobs, “Self-assembly of microscopic chiplets at a liquid-liquid-solid interface forming a flexible segmented monocrystalline solar cell.,” in *Proc. the National Academy of Sciences of the United States of America*, 2010, vol. 107, no. 3, pp. 993–8.

[25] K.-F. Bohringer, K. Goldberg, M. Cohn, R. Howe, and A. Pisano, “Parallel microassembly with electrostatic force fields,” in *Proc. IEEE International Conference on Robotics and Automation*, 1998, vol. 2, no. May, pp. 1204–1211.

[26] H. Ota, T. Araki, and M. Takeda, “Assembling process for microscopic components using magnetic force,” in *Proc. IEEE Tenth Annual International Workshop on Micro Electro Mechanical Systems*, 1997, pp. 209–214.

[27] K. Sato, K. Ito, S. Hata, and A. Shimokohbe, “Self-alignment of microparts using liquid surface tension—behavior of micropart and alignment characteristics,” *Precision Engineering*, vol. 27, pp. 42–50, 2003.

[28] T. Fukushima, E. Iwata, T. Konno, J.-C. Bea, K.-W. Lee, T. Tanaka, and M. Koyanagi, “Surface tension-driven chip self-assembly with load-free hydrogen fluoride-assisted direct bonding at room temperature for three-dimensional integrated circuits,” *Applied Physics Letters*, vol. 96, no. 15, p. 154105, 2010.

[29] T. Fukushima, E. Iwata, Y. Ohara, M. Murugesan, J. Bea, K. Lee, T. Tanaka, and M. Koyanagi, “Multichip self-assembly technology for advanced die-to-wafer 3-D integration to precisely align known good dies in batch processing,” *IEEE Transactions on Components, Packaging and Manufacturing Technology*, vol. 1, no. 12, pp. 1873–1884, Dec. 2011.

[30] T. Fukushima, T. Konno, E. Iwata, R. Kobayashi, T. Kojima, M. Murugesan, J.-C. Bea, K.-W. Lee, T. Tanaka, and M. Koyanagi, “Self-assembly ofchip-size components with cavity structures: high-precision alignment and direct bonding without thermal compression for hetero integration,” *Micromachines*, vol. 2, no. 1, pp. 49–68, Feb. 2011.

[31] Y. Y. Ong, Y. L. Lim, L. L. Yan, E. B. Liao, and V. Kripesh, “Dry self-assembly & gang bonding of micro-components from silicon carrier to substrate wafer,” in *Proc.Thirty-First IEEE/CPMT International Electronics Manufacturing Technology Symposium*, 2006, pp. 486–491.

[32] T. G. Leong, P. a Lester, T. L. Koh, E. K. Call, and D. H. Gracias, “Surface tension-driven self-folding polyhedra.,” *Langmuir: the ACS Journal of Surfaces and Colloids*, vol. 23, no. 17, pp. 8747–51, Aug. 2007.

[33] J. H. Cho, S. Hu, and D. H. Gracias, “Self-assembly of orthogonal three-axis sensors,” *Applied Physics Letters*, vol. 93, no. 4, p. 043505, 2008.

[34] T. G. Leong, B. R. Benson, E. K. Call, and D. H. Gracias, “Thin film stress driven self-folding of microstructured containers,” *Small*, vol. 4, no. 10, pp. 1605–9, Oct. 2008.

[35] J. Guan, H. He, D. J. Hansford, and L. J. Lee, “Self-folding of three-dimensional hydrogel microstructures,” *Journal of Physical Chemistry: Bhemistry. B*, vol. 109, no. 49, pp. 23134–7, Dec. 2005.

[36] R. R. A. Syms, “Surface tension powered self-assembly of 3-D micro-optomechanical structures,” *Journal of Microelectromechanical Systems*, vol. 8, no. 4, pp. 448–455, 1999.

[37] V. Sariola, Q. Zhou, and H. N. Koivo, “Hybrid microhandling: a unified view of robotic handling and self-assembly,” *Journal of Micro-Nano Mechatronics*, vol. 4, no. 1–2, pp. 5–16, May 2008.

[38] Q. Zhou and V. Sariola, “Unified view of robotic microhandling and self-assembly,” in *Robotic Microassembly*, M. Gauthier and S. Regnier, Ed. Wiley-IEEE Press, 2010, pp. 109–143.

[39] V. Sariola, M. Jääskeläinen, and Q. Zhou, “Hybrid microassembly combining robotics and water droplet self-alignment,” *IEEE Transactions on Robotics*, vol. 26, no. 6, pp. 965–977, 2010.

[40] V. Sariola, Q. Zhou, and H. Koivo, “Three dimensional hybrid microassembly combining robotic microhandling and self-assembly,” in *Proc. IEEE Int. Conf. Robotics & Automation*, 2009, pp. 2605–2610.

[41] M. Jaaskelainen, V. Sariola, and Q. Zhou, “Environmental effects on droplet self-alignment assisted hybrid microassembly,” in *Proc. IEEE International Symposium on Assembly and Manufacturing*, 2009, pp. 177–182.

[42] Q. Zhou, “Hybrid microassembly for 3D integration and heterogeneous integration of microsystem – EU FP7 Project FAB2ASM,” in *Proc. of Smart Systems Integration*, 2013.

[43] T. Young, “An essay on the cohesion of fluids,” *Philosophical Transactions of the Royal Society of London*, vol. 95, pp. 65–87, Jan. 1805.

[44] R. Wenzel, “Resistance of solid surfaces to wetting by water,” *Ind. Eng. Chem.*, vol. 28, no. 8, pp. 988–994, 1936.

[45] A. Cassie and S. Baxter, “Wettability of porous surfaces,” *Transactions of the Faraday Society*, no. 5, pp. 546–551, 1944.

[46] L. Gao and T. J. McCarthy, “How Wenzel and cassie were wrong,” *Langmuir: the ACS Journal of Surfaces and Colloids*, vol. 23, no. 7, pp. 3762–5, Mar. 2007.

[47] M. J. Hey and J. G. Kingston, “The apparent contact angle for a nearly spherical drop on a heterogeneous surface,” *Chemical Physics Letters*, vol. 447, no. 1–3, pp. 44–48, Oct. 2007.

[48] C. Extrand, “Model for contact angles and hysteresis on rough and ultraphobic surfaces,” *Langmuir*, vol. 1, no. 23, pp. 7991–7999, 2002.

[49] J. Oliver, C. Huh, and S. Mason, “Resistance to spreading of liquids by sharp edges,” *Colloids and Surfaces*, vol. 4, pp. 1–15, 1982.

[50] V. Liimatainen, V. Sariola, and Q. Zhou, “Controlling liquid spreading using microfabricated undercut edges,” *Advanced Materials*, Mar. 2013.

[51] T. Nishino, M. Meguro, K. Nakamae, M. Matsushita, and Y. Ueda, “The lowest surface free energy based on -CF 3 alignment,” *Langmuir*, vol. 15, pp. 4321–4323, 1999.

[52] K. A. Brakke, “The surface evolver,” *Experimental Mathematics*, vol. 1, no. 2, p. 391, 1992.

[53] A. Carlson, A. M. Bowen, Y. Huang, R. G. Nuzzo, and J. A. Rogers, “Transfer printing techniques for materials assembly and micro/nanodevice fabrication,” *Advanced Materials*, vol. 24, no. 39, pp. 5284–318, Oct. 2012.

[54] P. Lambert, M. Mastrangeli, J.-B. Valsamis, and G. Degrez, “Spectral analysis and experimental study of lateral capillary dynamics for flip-chip applications,” *Microfluidics and Nanofluidics*, vol. 9, no. 4–5, pp. 797–807, Mar. 2010.

Appendix: Publications

Aalto-DD 117/2013

ISBN 978-952-60-5261-8
ISBN 978-952-60-5262-5 (pdf)
ISSN-L 1799-4934
ISSN 1799-4934
ISSN 1799-4942 (pdf)

Aalto University
School of Electrical Engineering
Department of Automation and Systems Technology
www.aalto.fi

BUSINESS +
ECONOMY

ART +
DESIGN +
ARCHITECTURE

SCIENCE +
TECHNOLOGY

CROSSOVER

**DOCTORAL
DISSERTATIONS**